Rap1-dependent replication stress at telomeres induces relocalization to the Nuclear Pore Complexes

Mohamad Al Hajj, Manon Pierre, Marion Dubarry, Michael Chang, Vincent Géli, Dmitri Churikov, Marie-Noelle Simon

Rap1-dependent replication stress at telomeres induces relocalization to the Nuclear Pore Complexes.

Mohamad Al Hajj[1], Manon Pierre[1], Marion Dubarry[1,2], Michael Chang[3], Vincent Géli[1] and Dmitri Churikov[1#], Marie-Noelle Simon[1#]

1 Marseille Cancer Research Center (CRCM), U1068 Inserm, UMR7258 CNRS, Aix Marseille University, Institut Paoli-Calmettes, 27 bd Leï Roure, Marseille, France. Equipe labellisée Ligue Nationale contre le Cancer
2 present address : MAP Laboratory, INSA Lyon, Claude Bernard University UMR5240, Villeurbanne, France
3 European Research Institute for the Biology of Ageing, University Medical Center Groningen, Groningen, Netherlands

co-corresponding author: marie-noelle.simon@inserm.fr, dmitri.churikov@inserm.fr

Abstract

Nuclear pore complexes (NPCs) have emerged as a key structure in the spatial regulation of DNA damage repair, including at replication forks that are slowed down or stalled at various obstacles. Here, we show that interstitial telomeric sequence (ITS) and natural telomeres interact with the NPCs during their replication. This localization is entirely dependent on the tight binding of Rap1 as a modified ITS that poorly bind Rap1 does not interact with NPCs. As with other types of replication barriers, ITS localization to NPCs is dependent on Mre11 and on the SUMO pathway. In addition, we identified the PCNA loader Ctf18 as essential for ITS localization to NPCs, and showed that its function is mediated by Scc2-dependent *de novo* cohesin loading at the replication fork. We also found that Mrc1, which acts in the same *de novo* cohesin loading pathway as Ctf18, contributes to ITS localization to NPCs, independently of its checkpoint function. In addition, we uncovered a role for Sir4, which is involved in heterochromatin formation at telomeres, in the tethering of ITS to NPCs. We propose that localization to NPCs in S phase is initially triggered by single-stranded DNA at paused forks, which induces a SUMOylation wave, *de novo* cohesin loading and chromatin compaction. This, in turn, would limit resection, avoid checkpoint activation and possibly favor error-free restart of the replication fork.

INTRODUCTION

Telomeres are capping structures at the ends of linear chromosomes that protect them from degradation, harmful recombination, and end fusions. They are formed of G-rich repeated sequences that end up with a 3' single-strand overhang. Both single- and double-stranded telomeric DNA are bound by proteins that form the shelterin complex. In *S. cerevisiae*, telomeres are composed by approximately 300bp of irregular TG_{1-3} repeats and end up in a 12-14 nucleotide long 3' single-strand overhang. The Rap1 protein wraps double-stranded telomeric DNA to inhibit end fusion and recruits Rif1 and Rif2, which limit homologous recombination (HR) (Bonnell *et al*, 2021). The 3' overhang is bound by Cdc13, a subunit of the CST (Cdc13/Stn1/Ten1) complex. The conventional replication machinery cannot fully replicate the telomere ends, leading to an unavoidable shortening in the absence of a telomere maintenance mechanism (TMM). The one most widely used is based on telomerase, a specific reverse transcriptase that extends the 3' end overhang. The complementary strand is then synthetized by the conventional DNA polymerases. In the absence of telomerase, the telomeres progressively shorten at each replication cycle until they reach a critical length at which their capping functions become dysfunctional. Eroded telomeres are recognized as DNA damage that by activating the checkpoint, arrests the cell cycle and ultimately leads to senescence. Abrupt telomere shortening is another less understood source of short and/or dysfunctional telomeres. The repetitive nature of the telomeric sequence, its transcription, the tightly bound proteins of the shelterin complex, potential secondary structures such as the G-quadruplex or the t-loop, and finally the heterochromatin organization and silencing of subtelomeric regions all have the potential to interfere with replication fork progression at telomeres. As a consequence, a slowing or pausing of the replication fork has been observed in yeast (Ivessa et al, 2003; Makovets et al, 2004) and human (Verdun & Karlseder, 2006). Although this pause could be somehow beneficial to complete telomere replication, it is also at risk, requiring stabilization of the fork and is closely linked to the regulated requirement of DNA damage response factors in telomere length regulation (Bonnell *et al*, 2021). Indeed, proper processing of paused or stalled replication forks at telomeres is particularly crucial because non-replicated DNA at chromosome ends cannot be rescued by a convergent fork.

Because the telomerase is constitutively active in yeast and can efficiently solve replication issues, accessory factors involved in telomere replication in yeast are better identified in its absence. Upon inactivation of the telomerase, telomeres progressively shorten in yeast, as in human cells, and cells gradually lose their ability to grow, up to a permanent G2/M arrest, commonly defined as replicative senescence, in about 50-60 population doublings (Teixeira, 2013). Most notably, the kinetics of senescence - the rate at which the cell population loses its ability to grow - depends on a number of factors known to be involved in the response to replicative stress and/or the restart of stalled replication forks (Simon *et al*, 2016; Bonnell *et al*, 2021). Furthermore, in many cases, the accelerated senescence kinetics following inactivation of one of these factors does not directly correlate with an increased rate of telomere shortening at the telomere pool level. This suggests that appropriate fork stabilization and repair mechanisms are indeed required for accurate telomere replication and to prevent abrupt telomere shortening and/or deleterious accumulation of single-stranded DNA.

DNA transactions occur within a 3D-folded genome, which is organized in a compartmentalized nucleus. In this frame, telomere clusters are anchored to the nuclear periphery (NP) for most of the cell cycle through multiple tethering mechanisms involving telomere- and subtelomere-bound proteins and distinct NE-associated proteins (Taddei *et al*, 2010; Gasser & Stutz, 2023). Telomere tethering at the NP is functionally linked to subtelomeric gene silencing, telomere length regulation, and the regulation of DNA damage repair (Ebrahimi & Donaldson, 2008; Batté *et al*, 2017; Taddei *et al*, 2004; Therizols *et al*, 2006), but the contribution of these multiple anchoring pathways is poorly understood. At the nuclear periphery, nuclear pore complexes (NPCs) play a key role in the fate of various types of DNA damage, suggesting that they serve as a hub for specific molecular transactions at damaged sites, independently of their role in protein and mRNA trafficking in and outside of the nucleus (Simon *et al*, 2024). NPCs also function as scaffolds that influence chromatin states, nucleosome positioning, chromatin boundaries and, gene regulation (Sakuma & D'Angelo, 2017; Ptak & Wozniak, 2016). Relocalization of eroded telomeres to NPCs is coincident and contributes to recombination-dependent alternative TMMs, giving rise to survivors of telomerase inactivation (Khadaroo *et al*, 2009; Churikov *et al*, 2016; Charifi *et al*, 2021). Proper replication restart at fragile sites formed by non-B DNA structures or protein barriers is also highly dependent on the relocalization of stalled replication forks to NPCs (Su *et al*, 2015;

Kramarz *et al*, 2020; Whalen *et al*, 2020; Schirmeisen *et al*, 2024). A mutant of the nucleoporin Nup1 that prevents the relocation of stressed replication forks to NPCs, unleashes an error-prone restart mechanism at telomeres in the absence of telomerase (Aguilera *et al*, 2020). However, it remains unclear whether the translocation to NPCs is related to a defect in fork processing due to the absence of telomerase or represents a more general mechanism that contributes to the resolution of replicative stress at the telomeres.

In this study, we introduced telomeric repeats inside the genome to track a single well-defined locus and eliminate interferences related to telomerase action at chromosome ends. Using a modified telomeric sequence that poorly bind Rap1 as a control, we showed that tight Rap1 binding is the first trigger of replication fork stalling and telomere instability *in vivo*. As with other types of replication fork barriers, tight Rap1 binding at interstitial telomeric sequence (ITS) induces a relocalization to NPCs that depends on the remodeling of the loci during S phase.

RESULTS

Tight Rap1 binding acts as a roadblock to replication fork progression *in vivo*.

A wide range of telomere properties can slow or arrest the progression of the replication fork. Among them, it has been demonstrated that Rap1 bound to telomeric repeats, and not the telomere sequence per se, acts as a roadblock that inhibits distinct steps of telomere replication *in vitro* (Douglas & Diffley, 2021). Genetic and biochemical evidences suggest that Rap1 induces similar impediments to fork progression *in vivo* (Makovets *et al*, 2004; Goto *et al*, 2015). To further characterize this function and the pathway involved in overcoming this replication barrier, we introduced 300pb of telomeric repeats into chromosome VI adjacent to ARS607, a strong early origin of replication. This array was inserted in an orientation such that the G-rich strand is replicated by the lagging strand machinery, as occurs in natural telomeres (Figure 1A). Our design further removed the locus *YNCF001C*, which encodes one tRNA-Ala, because tRNA-coding sequences are known to induce replication stress and relocalization to NPCs (Ivessa *et al*, 2003; Chen & Gartenberg, 2014). In parallel, 300bp of a modified telomeric sequence lacking the G-triplet in the core binding site of Rap1 (GTGGGT) (Graham & Chambers,

1994; Lieb *et al*, 2001) was introduced at the same position (ITS-mod). Binding of Rap1 to each type of ITS was monitored by chromatin endogenous cleavage (ChEC), which is based on chromatin cleavage by micrococcal nuclease (MNase) fused to a protein of interest (Schmid *et al*, 2004). Cleavage is induced by the addition of Ca2+ to permeabilize cells, in which the intranuclear concentration of Ca2+ is too low to activate MNase. The efficiency and pattern of cleavage were monitored by Southern blotting of a 4,94kb restriction fragment containing the ITS insertion (Figure 1A and B). As shown in Figure 1B, within 30 s after Ca2+ addition, the intact *SfoI/ApaLI* fragment containing 300bp of telomeric sequence almost completely disappeared, and cleavage products were detected at the expected ITS position. These cleavage products are not detected when free MNase was expressed fused to an SV40 nuclear localization signal under the control of the *REB1* promoter (marked free-MN, Figure 1B) (Zentner *et al*, 2015). The same construct lacking the telomeric sequence (marked 0bp) introduced at the same position did not generate cleavage products, except at low levels within the *LSB3* promoter. Notably, the fragment containing the modified telomeric sequence (300bp-mod) was much more resistant to Rap1-MNase cleavage, suggesting that Rap1 binding was much looser in the absence of the GGG motif, as expected.

Accumulation of single-stranded (ss) DNA is a hallmark of compromised DNA replication at replication barriers. At telomeres, ssDNA is preferentially bound by the telomeric protein Cdc13 on the G-rich strand and RPA on the C-rich strand (Aguilera *et al*, 2020). In line with the observation that ITS impairs the progression of the replication fork (Makovets *et al*, 2004), we observed cleavage within the telomeric sequence upon the expression of a Cdc13-MNase fusion (Figure 1C and Figure S1A). Of note, in this experiment, the cleavage products were observed only after prolonged incubation with Ca^{2+} compared with Rap1-MNase, suggesting that only a fraction of the ITS in the cell population are accessible to Cdc13-MNase. Accordingly, no cleavage inside the ITS was observed when the cells were arrested in G1 following the addition of α-factor (Figure S1B). Prolonged incubation with Ca^{2+} also allowed to better visualize the accessibility of the locus to the free MNase, which cleaved the restriction fragment at several positions upstream and downstream of the ITS. Importantly, the free MNase expressed from the strong promoter Reb1 showed no cleavage inside the ITS. Taken together, our data suggest that Cdc13 specifically binds to the ITS in a fraction of cells. A similar result was observed following the expression of a Rfa1-MNase fusion (Figure 1D). For both Rfa1 and Cdc13, no cleavage was detected inside the ITS-mod (Figure 1C, D). This result

indicates that telomeric repeats but not modified repeats generate replication stress with consecutive accumulation of ssDNA. In line with *in vitro* observations (Douglas & Diffley, 2021), it appeared that neither the telomeric sequence nor the presence of Rap1 is an impediment during DNA replication unless Rap1 tightly binds and wraps the telomeric sequence, forming a strong roadblock to fork progression. These observations are concordant with the differential role of Rap1 in regulating telomere length, depending on its DNA binding mode (Bonetti *et al*, 2020).

Rap1-dependent replication fork arrest induces relocalization to the NPCs.

Increasing evidence suggest a role for NPCs in handling and/or restarting stalled replication forks in both yeast and human cells (Simon et al., 2024). We next asked whether interstitial telomeric sequences also relocalize to the NP and/or NPCs in a Rap1-dependent manner. As a first step, we determined whether the ITS were tethered to the NP as natural telomeres. For this purpose, we used a strain in which the ARS607 locus could be visualized *in vivo* through the binding of a LacI*-GFP protein fusion to an array of LacOp repeat arrays placed upstream of the ARS607 (Figure 2A). The position of the locus in the nucleus was scored relative to the nuclear periphery, which was marked by the nucleoporin GFP-Nup49 and binned into three concentric zones of equal volumes as described (Meister *et al*, 2010) (Figure 2A). Strikingly, although the locus containing the ITS was evenly distributed among the three zones in cells in the G1 and late S phases, it was transiently enriched at the NP, specifically in the early S phase, consistent with the firing of ARS607 early in S phase (Friedman *et al*, 1997) (Figure 2A and Figure S2) . We concluded that interstitial telomeric sequences do not possess the characteristics required for attachment to the NP in G1, as observed for natural telomeres, but undergo transient relocalization coincident with their replication.

We then investigated whether ITS induces relocalization of the locus to the NPCs. For this, nucleoporins were tagged with MNase at native locus. We found that the locus devoid of ITS is poorly accessible to MNase cleavage when using a fusion with the Y complex nucleoporin Nup84 (see 0bp), several cleavage products are detected upon the introduction of 300bp of telomeric repeats (Figure 2B). The main cleavage sites were concentrated just upstream and downstream of the ITS as well as to a lesser extent inside the telomeric repeats (Figure 2B and Figure S3A). In contrast, the cleavage sites close to and inside the ITS were not accessible by

free MNase. Similar results were obtained when the nuclear basket protein Nup2 fused to MNase was expressed in place of Nup84-MNase (Figure S3B). With both Nup84- and NUP2-MNase, cleavage of the locus was greatly decreased when the ITS was replaced by the ITS-mod, and no cleavage was observed either just close or inside the ITS-mod (Figure 2C and S3C). Cleavage inside a region corresponding to the *LSB3* promoter was also increased upon introduction of the ITS (compare 300bp and 300bp-mod in figure 2C and Figure S3C) suggesting that the entire locus was in close proximity to the NPCs. Contact of the ITS-containing locus with NPCs appeared independent of Mps3 integrity, a nuclear envelop protein that anchor telomeres at the NP during S phase (Figure S3D) (Gasser & Stutz, 2023). Because telomere repeats induce telomere instability in both orientations (Aksenova *et al*, 2013, 2015), we next wondered whether the relocalization of the interstitial telomeric sequence to NPCs relies on strong blockage when the convergent fork reach the ITS. Distal to the ITS, the replication origins ARS608 and ARS609 are located 17 and 57kb from ARS607, respectively. However, the double deletion of ARS608 and ARS609 did not impact the cleavage around and inside the ITS by Nup2-MNase (Figure S5D). Together, our data suggest that paused replication forks generated by tight binding of Rap1 lead to NPC association, similarly to what has been described for other types of replication barriers (Horigome *et al*, 2019; Su *et al*, 2015; Kramarz *et al*, 2020).

We next tested whether natural telomeres also relocalize to the NPCs. For most of the cell cycle, telomeres cluster at the NP though interactions with several proteins of the nuclear membrane (Gasser & Stutz, 2023) , making it difficult to distinguish interactions with the NPCs from other types of anchors at the NP. For this reason, we used ChEC to monitor whether telomere repeats directly contact the NPCs. Fusion between either Nup2 or Nup84 with micrococcal nuclease cleaved just upstream of the telomeric sequences (Figure 3A). No cleavage was observed using a Nic96-MNase fusion, in line with its position in the inner ring complex of the NPCs (Beck & Hurt, 2017). Much less cleavage was observed upon the expression of free MNase as compared with Nup2 and Nup84-MNase (Figure 3A). Finally, none of Nup-MNase fusions cleaved significantly a control locus (Figure S4A). Noteworthy, only Nup2-MNase also showed some cleavage within the duplicated subtelomeric Y' sequences (red square, Figure 3A), as expected from its enrichment at subtelomeres and its role in demarcating the boundaries between active and silenced chromatin (Dilworth *et al*, 2005). Finally, the cleavage of telomeres by Nup84-MNase is not abrogated by inactivating the two

main pathways involved in the anchoring telomeres to the nuclear periphery (Taddei *et al*, 2004) either through deletion of *ESC1* or upon expression of the *mps3Δ65-145* allele (Figure 3B and Figure S4B). Together with our previous publication (Aguilera *et al*, 2020), these new data suggest that at least a fraction of telomeres transiently localize to the NPCs regardless of whether the telomerase is active or not.

The MRX complex and the SUMO pathway are involved in the localization of interstitial telomeric sequences to NPCs.

Previous publications have provided detailed requirements for relocalization to the NPCs of replication forks stalled at protein barriers or DNA structure-forming sequences emphasizing the involvement of the SUMO pathway, recombination factors, and resection (Whalen *et al*, 2020; Kramarz *et al*, 2020) in a model very similar to that described for the relocalization of hard-to-repair double-strand breaks (DSBs) (Nagai *et al*, 2008), eroded telomere (Churikov *et al*, 2016; Charifi *et al*, 2021) and, more recently, R-loop-forming loci (Penzo *et al*, 2023). However, the presence of telomeric repeats has been shown to alter the processing of damage, biasing the choice of repair pathway (Marcomini *et al*, 2018; Stivison *et al*, 2020). Therefore, we initiated a candidate approach to identify mutations that interfere with the relocalization of ITS to NPCs. The repair proteins Rad5 and Rad51 appeared to be dispensable for tethering to NPCs as well as the recombination factor Rad59, which is involved in homeologous recombination (Figure S5A). In contrast, *MRE11* deletion reduced the interaction with NPCs (Figure S5B). To better quantify this defect, we coupled ChECs to qPCR amplification of the cleavage products. Figure 4A shows the rationale for the ChEC-qPCR assay. This approach further confirmed that deleting *MRE11* decreased the efficiency of ITS cleavage by Nup2-MNase (Figure 4B).

The DNA damage response induces a wave of protein mono- and poly-SUMOylations that create binding sites for SUMO-dependent ubiquitin ligases (STUbL) (Psakhye & Jentsch, 2012; Gasser & Stutz, 2023a). The STUbL Slx8/Slx5 plays a key role in anchoring DSBs, arrested forks and R-loops to NPCs, possibly by directly interacting with Nup84 (Nagai *et al*, 2008; Su *et al*, 2015; Penzo *et al*, 2023). Yet, the relocalization of DSBs flanked by telomeric repeats depends on the STUbL Uls1, which may promote Rap1 degradation at the NPCs (Marcomini *et al*, 2018). Deletion of *ULS1,* however, did not affect ITS relocalization to NPCs (Figure S5C). This

may be because there are actually very few breaks in the telomeric sequence during replication. In contrast, *SLX8* deletion reduced cleavage by Nup2-MNase in the ChEC assay (Figure 4B and S5C). This is consistent with the consensus model in which damage-induced SUMOylation events generate binding sites for STUbL for its relocalization to NPCs (Simon *et al*, 2024). Accordingly, deletion of the C-terminal domain of the SUMO E3 ligase Mms21, which abolishes its SUMO-ligase activity (Zhao & Blobel, 2005), also decreased contact between the ITS locus and NPCs (Figure 4B and S5B). ITS cleavage by Nup2-MNase was slightly impaired when Rad52 SUMOylation was prevented by the expression of the *rad52-3KR* allele (Sacher *et al*, 2006) (Figure S5C). This suggests that in order to create the SUMO-enriched environment required for relocalization to NPCs, other factors must be SUMOylated in addition to Rad52. Nevertheless, Nup2-MNase cleavage was unaffected in the *rfa1-4KR* mutant, which largely eliminates RPA SUMOylation (Dhingra *et al*, 2019) (Figure S5D). This contrasts with the role of RPA SUMOylation in the relocalization of GAC triplet repeats (Whalen *et al*, 2020) and R-loops (Penzo *et al*, 2023) to NPCs and suggests specific requirements at telomeres that may be related to competition between RPA and Cdc13 for binding telomeric single-stranded DNA.

Sir4 contributes to localization of ITS to NPCs.

The proteins Sir4 and Sir3 are among the main interactors of Rap1 (Moretti P et al., 1994, Marcand et al. 1996). They participate in major pathways of telomere anchoring to the NP and mediate, with the histone deacetylase Sir2, silencing at telomeres (Kueng *et al*, 2013). In addition, it has been reported that replication stress due to tight replication barriers induces recruitment of the SIR complex to favor heterochromatin-like structures and promotes relocalization to the NP (Dubarry *et al*, 2011; Nikolov & Taddei, 2016). Interestingly, Sir4 was shown to interact with a structurally distinct variant of the NPC, called SNUP, which lacks components of the nuclear basket and inner ring (Lapetina *et al*, 2017) and promotes the anchoring of telomeres to the NP (Van de Vosse *et al*, 2013; Lapetina *et al*, 2017). We found that *SIR4* deletion reduced ITS cleavage by Nup84-MNase (Figure 5B). A similar result was obtained with Nup2-MNase (Figure S6A). Nevertheless, although the SNUP variant has been implicated in telomere silencing (Van de Vosse *et al*, 2013; Lapetina *et al*, 2017), the interstitial telomeric sequence did not silence the flanked *URA3* gene (Figure S6B).

Among nucleoporins, Nup170 physically interacts with Sir4 and Rap1, and binds cooperatively with them to subtelomeric DNA, which is essential for tethering to nuclear envelope in G1 phase and for subtelomeric gene silencing (Van de Vosse *et al*, 2013). Although Nup170 seems dispensable for telomere localization to nuclear periphery in S phase (Van de Vosse et al., 2013), it may be explained by redundancy of the localization pathways acting in S phase (Hediger et al., 2002). Therefore, we tested the role of Nup170 in localization of the ITS to NPCs, knowing that ITS localization occurs specifically during its replication in S phase. We found that *NUP170* deletion only moderately affected the cleavage of ITS by Nup84-MNase (Figure S7A), which is consistent with a notion that Nup170 is not solely responsible for ITS localization to NPCs in the S phase.

Ctf18 function in *de novo* cohesin loading is required for ITS localization to NPCs

Recently, Aitchison laboratory has shown that Ctf18, the large subunit of the alternative PCNA loader, interacts with NPCs in S phase (Choudhry et al., 2023). This prompted us to test whether Ctf18 plays a role in localization of ITS to NPCs. To our surprise, we found that deletion of *CTF18* nearly abolished ITS cleavage by Nup84-MNase (Figures 5B and S7C). Since both Nup170 and Ctf18 are required for maintaining the level of PCNA on chromatin by acting in the same pathway (Choudhry et al., 2023), we reckoned that yet another function of Ctf18 is responsible for much stronger effect of its inactivation on ITS localization to NPCs.

In addition to PCNA loading, the Ctf18-RFC complex plays key roles in the establishment of sister chromatid cohesion (Hanna et al., 2001) and S phase checkpoint activation (García-Rodríguez et al., 2015). To assess whether Ctf18 function in *de novo* cohesin loading (Murayama et al., 2018; Srinivasan et al., 2020) is involved in ITS localization to NPCs, we took advantage of the temperature-sensitive (ts) allele of the cohesin loader Scc2 (Petela et al., 2018). In the *scc2-45* ts strain, the ITS cleavage by Nup84-MNase was significantly reduced at semi-permissive temperature (Figure 5B) pointing to the role of cohesion establishment during DNA replication for localization to NPCs. Partial reduction of ITS cleavage by Nup84-MNase in the *scc2-45* strain, possibly due to incomplete inactivation of Scc2, precluded us from drawing a conclusion that a profound effect of *CTF18* deletion is related entirely to the defect in *de novo* cohesin loading. Therefore, we sought another way to address this question.

Previous genetic analysis uncovered two epistasis groups of genes/proteins involved in parallel sister chromatid cohesion establishment pathways in S phase: one independent and another dependent on cohesin loader Scc2, named "cohesin conversion" and "*de novo* loading", respectively (Xu et al., 2007; Srinivasan et al, 2020). Ctf18 and Mrc1, also known for its role in S-phase checkpoint, belong to the same *de novo* cohesin loading pathway. Thus, we examined the effect of *MRC1* deletion on ITS localization to NPCs. In accord with our expectation, deletion of *MRC1* also reduced ITS cleavage by Nup84-MNase (Figure 5C) albeit to a lesser extent compared to that of *CTF18* deletion. Since both Mrc1 and Ctf18 are non-redundantly involved in activation of the S-phase checkpoint, we also tested checkpoint-defective *mrc1-AQ* allele (Osborn and Elledge, 2003) to verify whether replication checkpoint plays any role in localization of ITS to NPCs. We found that inactivation of the S-phase checkpoint function of Mrc1 did not have any measurable effect on ITS localization to NPCs (Figure 5C). Together, these results strongly suggest that Ctf18 and Mrc1 functions in ITS localization to NPCs are mediated by their involvement in *de novo* cohesin loading during DNA replication (Srinivasan et al, 2020; Shrestha et al., 2023). Given a stronger effect of *CTF18* deletion compared to that of *MRC1*, we consider that maintenance of the balanced PCNA level at the replication fork by Ctf18 may also play a role. At the moment, the latter issue is difficult to disentangle since PCNA also contributes to *de novo* cohesin loading by recruiting Scc2 (Psakhye et al., 2023).

Rap1 binding impacts the stability of telomeric repeats.

ITS are inherently highly unstable (Aksenova *et al*, 2013; Goto *et al*, 2015). To further determine whether this is dependent on the tight binding of Rap1, we first monitored whether ITS and ITS-mod are prone to expansion or contraction (stability assay, Figure 6A). Starting with a single clone, the length of the ITS was analyzed using PCR with ITS flanking primers in its progeny after a limited number of cell divisions (see Materials and Methods). No variation in the length of the ITS-mod was detected under these conditions, demonstrating the ability of the canonical replication machinery to faithfully replicate TG repeats. In contrast, approximately 1% of the progeny from ITS carrying clones showed either an expansion or a contraction of the ITS length (Figure 6B). ITS sequence analysis of some of these clones revealed that expansions and contractions corresponded, respectively, to short internal

duplications or deletions within the first 150 bp of the ITS sequence (Figure S8A). This result ruled out the possibility of recombination with natural telomeres. Instead, it suggests that sister-chromatid exchange occurs as the restarted replication fork progresses in the telomeric sequence. Inactivation of the repair factor Rad5 further increased ITS instability about three-fold, indicating that the template switch-dependent repair pathway is important for maintaining the integrity of the telomeric sequences during replication. Surprisingly, deleting *MRE11* stabilized ITS length with a lower incidence of expansions and contractions (Figure 6B). MRX promotes resection at stalled replication forks in several ways (Delamarre *et al*, 2020; Teixeira-Silva *et al*, 2017). Our results thus suggest that, unlike other types of protein barriers and CAG repeat DNA-forming structures (Kramarz *et al*, 2020; Sundararajan *et al*, 2010), ssDNA accumulation is detrimental to replication fidelity at telomeric repeats. Noteworthy, deletion of *SIR4* or *CTF18* that both impair localization of the ITS to the NPCs had no effect on ITS stability (Figure 6B).

To further determine whether the ITS also induces DNA breaks in a Rap1-dependent manner, we set up a fragility assay (Figure 6C). For this, both the ITS and ITS-mod were integrated 13 kb from the strong replication origin ARS922. At this position, the distal 15 kb chromosome fragment can be lost without affecting cell viability. The *ADE2* gene was inserted downstream of the ITS to monitor the loss of the terminal fragment (red *ade2* minus cells) (Figure 6C). Starting with a single white clone, we monitored the number of colonies with, at least, on red sector (ade minus cells) in its progeny after a limited number of cell divisions (see Materials and Methods). No red sectors were detected in colonies of cells carrying the ITSmod, whereas about 5% of colonies carrying the wild type ITS had a red sector. (Figure 6D). Sequencing of the terminal fragment after amplification by teloPCR (Förstemann *et al*, 2000) showed that indeed the red colonies lost the chromosome end downstream of the ITS (and hence the *ADE2* gene) and generate de novo telomeres from inside the ITS probably through elongation by the telomerase (Figure S8B).

Once again, the MRX complex appeared to be a key player, as deletion of *MRE11* led to a significant reduction in the appearance of red cells (Figure 6D). However, this result should be interpreted with caution as Mre11 binding to TG repeats is required for telomerase recruitment and efficient telomerase-dependent elongation (Negrini *et al*, 2007). Nevertheless, ssDNA protection appeared important to prevent ITS fragility as defective ssDNA protection upon expression of the *rfa1-D228Y* allele (Schmid *et al*, 2004; Audry *et al*, 2015),

increases the frequency of ITS instability (Figure 6D). Surprisingly, the deletions of *RAD5* which is implicated in recombination-dependent restart of stalled forks, did not affect ITS fragility. ITS fragility was deeply decreased upon deletions of *SIR4* or *CTF18*. Reduced ITS fragility may have several roots. First, the survival of *ade-* cells in this setting depends on the ability to generate or maintain a telomere at the end of the break. This step might be prevented by mutations affecting telomerase activity, as discussed above for *mre11Δ* cells. Consistent with this first possibility, *ctf18* and *sir4* deleted cells, but not *nup170* cells, exhibited shorter telomeres, although to a lesser extent than *tel1* or *ku* mutants (Figure 7A). Alternatively, breaks that occur upstream or at the beginning of the ITS may leave less than the 34bp required for efficient *de novo* telomere initiation (Strecker *et al*, 2017). At natural telomeres, these breaks would abruptly shorten telomeres, accelerating senescence in the absence of telomerase (Martin *et al*, 2021). Along this lines, inactivation of *MRC1*, *SIR4* and *SLX8*, all of which impact localization to the NPCs, also accelerates senescence (Grandin & Charbonneau, 2007; Kozak *et al*, 2010; Azam *et al*, 2006; Charifi *et al*, 2021). The same holds true for *CTF18* and *MMS21* whose inactivation also greatly accelerated senescence (Figure 7B and C).

DISCUSSION

Accurate telomere replication is the lynchpin of telomere length regulation. Nevertheless, this process is at risk because of the many intrinsic challenges that the replication machinery encounters at telomeres. In addition to the “end replication problem”, telomeres are prone to various types of roadblocks that can hamper replication fork progression. Although these potential obstacles have been well documented, there is still little understanding whether they can individually slow or pause the replication fork, and how they are resolved at the cellular level. Here, we used TG repeats which are differentially bound by Rap1 to demonstrate that the tight binding of Rap1 to telomeric repeats has detrimental consequences for the accuracy of DNA replication, in agreement with the inhibitory role of Rap1 *in vitro* (Douglas & Diffley, 2021) and fork pausing at telomere sequence *in vivo* (Makovets *et al*, 2004; Goto *et al*, 2015). We previously showed that the ssDNA-binding proteins Cdc13 and Rfa1 colocalize in foci in S/G2 (Khadaroo *et al*, 2009). Although these foci are only detectable at a low frequency, their abundance increases after telomerase inactivation, well before the cells enter senescence (Khadaroo *et al*, 2009; Aguilera *et al*, 2020).

However, the question remained whether these foci were due to DNA degradation of telomere ends, possibly linked to the regeneration of the 3'-overhang (Faure *et al*, 2010), or whether they marked internal ssDNA gaps. By placing telomeric sequences internally in the genome, we now show that the presence of ssDNA bound by Cdc13 and RPA is linked to the replicative stress induced by Rap1 binding. Accumulation of ssDNA at stalled replication forks is a hallmark of replicative stress and is necessary for fork restart (Delamarre *et al*, 2020). However, its production needs to be carefully regulated because of its propensity to break down and to promote large chromosomal rearrangements (GCR) (Tye *et al*, 2021). This could be of major importance for repeated sequences in which faulty annealing events are a potential source of duplications or deletions (Aguilera *et al*, 2020). In this context, we showed here that deletion of *MRE11,* which plays a key role in ssDNA production through various mechanisms (Delamarre *et al*, 2020), tends to reduce the basal level of instability and fragility at the ITS.

Importantly, we found that both ITS and natural telomeres transiently interact with NPCs. This finding corroborates our previous observations in cells lacking telomerase (Aguilera *et al*, 2020) and further demonstrates that this mechanism is not a secondary consequence of the absence of telomerase. This finding reinforces the role of transient localization of stalled replication forks to NPCs in replication fork handling, a mechanism that, although not yet fully understood, seems to be conserved from yeast to humans (Simon *et al*, 2024; Pinzaru *et al*, 2020; Rivard *et al*, 2024). As observed with other types of replication barriers, ITS relocalization to NPCs depends on remodeling of the stalled fork via the SUMO pathway and resection (Whalen *et al*, 2020; Kramarz *et al*, 2020). Furthermore, we detected a severe defect in the absence of Ctf18, which is consistent with the recent discovery of the recruitment of the Ctf18-RFC complex to a subpopulation of NPCs (Choudhry *et al*, 2023). The similar defect observed upon inactivation of *MRE11* and *CTF18* suggests that they may act via a common pathway. The Ctf18-RFC complex is multifunctional in maintaining genome stability, including through PCNA loading and promotion of sister chromatid cohesion during replication (Liu *et al*, 2020; Srinivasan *et al*, 2020; Psakhye *et al*, 2023). Similarly, the MRX complex cooperates with chromatin modifiers to promote resection and cohesin loading at stalled replication forks (Tittel-Elmer *et al*, 2009; Delamarre *et al*, 2020). The impact of *mrc1* and *scc2-45* mutations on ITS relocalization to NPCs further argues for a role of de novo cohesin loading at stalled fork in this pathway. The link between *de novo* cohesin loading behind the fork and localization to NPCs is tantalizing. Given cohesin's ability to spatially organize chromatin via its loop extrusion

activity, it is possible that localization to NPCs may result from such cohesin activity. Future studies that take advantage of the cohesin loop extrusion mutants would be essential to make advances in this direction. Relocalization to the NPCs ensures efficient recombination-dependent restart of replication forks stalled at protein barriers (Schirmeisen *et al*, 2024). Cohesin loading may also contribute to fork restart by facilitating template switch with the sister chromatid via the Rad18/Rad5 pathway (Tittel-Elmer *et al*, 2009; Fumasoni & Murray, 2020; Litwin *et al*, 2018).

Surprisingly, we further revealed the key role for Sir4 in the tethering and/or anchoring of replication forks stalled at ITS to NPCs. Sir4 is known for its role in silencing and telomere cluster formation at the NP through its interaction with Esc1, a protein associated with the inner nuclear membrane (Gasser & Stutz, 2023). Esc1 also interacts with the nuclear pore variant SNUP, but the Nup170-Esc1-Sir4 axis is important for telomere anchoring at the NP in G1 (Van de Vosse *et al*, 2013). Nevertheless, in addition to its role in silencing specific regions of the genome, the Sir complex is recruited at DSBs and replication pause sites (Mills *et al*, 1999; Bordelet *et al*, 2022; Dubarry *et al*, 2011). This emerges as a general mechanism, because despite the general chromatin decondensation induced by DNA damage, heterochromatin factors are also transiently recruited to DNA damage sites in human cells (Lemaître & Soutoglou, 2014; Gaggioli *et al*, 2023). The role of this transient recruitment of silencing factors remains unclear. Sir proteins may be important for limiting resection and ssDNA accumulation, thereby dampening checkpoint activation. Supporting this hypothesis, Sir3 limits Mre11-mediated resection at DSBs in a manner that is in part independent of its heterochromatin-promoting function (Bordelet *et al*, 2022). Silent chromatin also suppresses checkpoint activation in rDNA under replication stress (Bentsen *et al*, 2013). Not exclusively, recruitment of the Sir complex could inhibit homologous recombination and promote error-free restart of the replication fork. Consistent with this possibility, Sir4 deficiency enhances subtelomeric recombination (Liu *et al*, 2020), and Sir3/Sir4 inhibits the early steps of HR in vitro (Sinha *et al*, 2009). Finally, the Sir complex may function in parallel with Ctf18-RFC in loading or maintaining cohesin to stalled replication forks (Chang *et al*, 2005). Although it has been proposed that replisome impediments may play a role in establishing and maintaining silencing (Dubarry *et al*, 2011; Nikolov & Taddei, 2016), no silencing was detected at the *URA3* gene flanking the ITS (Figure S6B) and the ITS were not preferentially enriched at the NP in G1 (Figure 2A). This is in strong contrast to natural telomeres where Ctf18, Sir4 and Nup170 are

required for silencing and NP anchoring, mainly in G1 (Hiraga *et al*, 2006; Van de Vosse *et al*, 2013). From our data, we propose that silencing might be initiated during telomere replication but requires additional actor(s) or feature(s) of natural telomeres to permanently establish heterochromatin and promote telomere clustering and anchoring to the NP.

The role of transient telomere localization to NPCs remains a key question. Although cells lacking *CTF18*, *SIR4,* or *MRE11* all have short telomeres, it is premature at this stage to establish a direct correlation between telomere length and NPC anchoring, as telomerase recruitment itself involves many factors. In this regard, other mutations affecting NPC localization, such as *mms21-1* and *slx8*, have either no or opposite effects on average telomere length in the presence of telomerase (Azam *et al*, 2006; Zhao & Blobel, 2005). In the absence of telomerase, however, all the mutations affecting relocalization to NPCs (*slx8*, *mms21ΔCt*, *sir4*, *ctf18*, *mrc1*) accelerate senescence, as does the inactivation of proteins involved in fork restart but not required for relocalization to NPCs (*rad51*, *rad5*) (Grandin & Charbonneau, 2007; Kozak *et al*, 2010; Azam *et al*, 2006; Charifi *et al*, 2021; Fallet *et al*, 2014; Le *et al*, 1999). One notable exception is *MRE11* whose deletion impacts relocalization to the NPCs but slows down senescence (Ballew & Lundblad, 2013). From all these data, it is thus tempting to speculate that Mre11-dependent accumulation of ssDNA at stalled fork is the first signal for NPC relocalization by inducing a wave of SUMOylation, de novo cohesin loading and chromatin compaction in order to fine regulate ssDNA level and prevent checkpoint activation. In this scenario, it is possible that deleting *MRE11* bypass the requirement for NPC relocalization to stabilize the fork, as suggested by the role of Mre11 in accelerating senescence.

Materials and Methods

Yeast strains

Strains used in this study are described in Supplementary Table 1. Strains were constructed and analyzed by standard genetic methods.

Senescence assays

Liquid senescence assays were performed starting with the haploid spore products of diploids that were heterozygous for *EST2* (*EST2*/*est2Δ*) and for the gene(s) of interest. To ensure homogeneous telomere length before sporulation, the diploids were propagated for at least 50 PDs on YPD plates. After 3 days of growth at 30°C, the entire spore colonies were transferred to 2ml liquid YPD to estimate the number of PDs and the suspension immediately diluted to

10^5 cells per ml. Cells were serially passaged in 15 ml liquid YPD medium at 10^5 cells per ml at 24h intervals. Replicative senescence curves shown in this study correspond to the average of several independent spores with identical genotype.

TeloPCR:

de novo telomeres were amplified by PCR using the AccuPrime™ GC-Rich DNA Polymerase (InVitrogen) after TdT-dependent addition of a poly C tail at the end (Förstemann *et al*, 2000) using a primer located upstream of the *URA3* gene and a polyG(A/C) primer. The PCR fragment was sequenced by Eurofins Genomics. The point of divergence was defined when the sequence could not be aligned with the ITS sequence.

Stability and fragility assays.

Single colonies carrying 300pb of ITS or ITSmod were recovered in 2ml YPD medium, grown to saturation at 30°C (six to seven population doublings) to allow for expansion, contraction and breaks and plated on YPD. For the instability assay, colony PCRs were performed on single colonies and analyzed on 2% agarose gels. For the fragility assay, the number of colonies presenting one or several red sectors were monitored.

ChEC and ChEC-qPCR

ChEC experiments have been performed according to published protocol (Zentner et al., 2015). Briefly, the cells were harvested by centrifugation from 50 mL of log phase cultures in YPD and washed three times with 1 mL Buffer A (15 mM Tris-HCl, pH 7.5, 80 mM KCl, 0.1 mM EGTA) supplemented with EDTA-free protease inhibitors, 0.2 mM spermine, and 0.5 mM spermidine. Then, cells were permeabilized by resuspending in 600 µl of Buffer A supplemented with 0.1% digitonin and 1 mM PMSF. After 5 minutes at 30°C, $CaCl_2$ solution was added to 2 mM final concentration to activate endogenous MNase fusion protein. The 150 µl aliquots corresponding to cleaved chromatin were transferred to the tubes prefilled with the equal volume of 2x Stop solution (400 mM NaCl, 20 mM EDTA, 4 mM EGTA and 2% SDS) to inactivate MNase at the desired time points. At the end of the experiment, 3 µl of the 20 mg/ml Proteinase K was added to each aliquot to digest bulk protein at 55°C for 20 min. DNA was extracted using standard phenol/chloroform (pH 8.0) method.

The DNA was stained with selective dsDNA dye (Broad-Range) and its concentration was measured using Qubit fluorometer. In preparation for adapter ligation, 400 µg of each DNA sample was treated with T4 Polynucleotide Kinase (T4 PNK) in the presence of 1 mM ATP to both remove the phosphate from the 3' end generated by MNase cleavage and to

phosphorylate the 5' end of DNA. An aliquot of T4 PNK-treated DNA was then incubated with Taq polymerase in the presence of 0.2 mM dNTPs and 1.5 mM Mg^{2+} ions to both fill-in the recessive DNA ends generated by MNase and to add the dA tail to the 3' DNA end to facilitate adapter ligation. The partially double-stranded DNA oligonucleotide adaptor with the 3' dT tail and the longer 5' overhang on the other end was then ligated to the DNA pre-treated with T4 PNK and Taq polymerase to generate a primer binding site for PCR amplification of the MNase cleavage products. The adapter-ligated DNA was then diluted to 250 pg/µl, and 1 µl of each DNA was used to amplify the ligation junction in 10 µl of the Takara SYBR Green qPCR mix using one primer complementary to the ligated adapter and another one complementary to the DNA sequence adjacent to the ITS site in the genomic DNA. The relative quantity of the qPCR product was determined using the standard curve method implemented in the Rotor-Gene qPCR analysis software. All samples were analyzed in triplicates. Raw cleavage efficiencies were normalized to the amplification level of the *ARO1* locus.

Detailed ChEC qPCR protocol (including the adapter oligonucleotides and primer sequences) is available on request.

Southern blot

DNA from ChEC experiments was analyzed by Southern blotting followed by hybridization with ^{32}P-labelled probe as previously described (Churikov *et al*, 2014). The primer sequences used to generate the probe for the ARS607/ITS locus are available on request.

Zoning assay

Cells were then grown over-night at low density on YPD plates supplemented with adenine before imaging. Observations were performed using a Nikon Eclipse Ti microscope with a x100 objective and a binning x2. Cell images were captured with a Neo sCMOS Camera (Andor) as Z-stack of 21 images with a step interval of 0.2um. The zoning assay was then performed using median filtered LacI-GFP and GFP-NUP49 stacks using the point-picker plugin in ImageJ software (Meister *et al*, 2010). G1, early and late S phase were defined as cells with no, tiny and medium buds respectively.

ACKNOWLEDGMENTS

We thank Kim Nasmyth for sharing the *scc2-45* strain. MAJ was supported by La Ligue Nationale contre le Cancer contre le Cancer (ARC). M.D was supported by the Agence Nationale de Recherche (ANR-19-CE12-0023 NIRO). M. P. was supported by the Agence

Nationale de Recherche (ANR-23-CE12-0007). V.G. was supported by the Ligue Nationale Contre le Cancer (Equipe labellisée). This work is funded by the Agence Nationale de Recherche (ANR-19-CE12-0023 NIRO and ANR-23-CE12-0007 SpaceForkIn to MNS)

references

- Aguilera P, Whalen J, Minguet C, Churikov D, Freudenreich C, Simon M-N & Géli V (2020) The nuclear pore complex prevents sister chromatid recombination during replicative senescence. *Nat Commun* 11: 160
- Aksenova AY, Greenwell PW, Dominska M, Shishkin AA, Kim JC, Petes TD & Mirkin SM (2013) Genome rearrangements caused by interstitial telomeric sequences in yeast. *Proc Natl Acad Sci U S A* 110: 19866–19871
- Aksenova AY, Han G, Shishkin AA, Volkov KV & Mirkin SM (2015) Expansion of Interstitial Telomeric Sequences in Yeast. *Cell Rep* 13: 1545–1551
- Audry J, Maestroni L, Delagoutte E, Gauthier T, Nakamura TM, Gachet Y, Saintomé C, Géli V & Coulon S (2015) RPA prevents G-rich structure formation at lagging-strand telomeres to allow maintenance of chromosome ends. *EMBO J* 34: 1942–1958
- Azam M, Lee JY, Abraham V, Chanoux R, Schoenly KA & Johnson FB (2006) Evidence that the S.cerevisiae Sgs1 protein facilitates recombinational repair of telomeres during senescence. *Nucleic Acids Res* 34: 506–516
- Ballew BJ & Lundblad V (2013) Multiple genetic pathways regulate replicative senescence in telomerase-deficient yeast. *Aging Cell* 12: 719–727
- Batté A, Brocas C, Bordelet H, Hocher A, Ruault M, Adjiri A, Taddei A & Dubrana K (2017) Recombination at subtelomeres is regulated by physical distance, double-strand break resection and chromatin status. *EMBO J* 36: 2609–2625
- Beck M & Hurt E (2017) The nuclear pore complex: understanding its function through structural insight. *Nat Rev Mol Cell Biol* 18: 73–89
- Bentsen IB, Nielsen I, Lisby M, Nielsen HB, Gupta SS, Mundbjerg K, Andersen AH & Bjergbaek L (2013) MRX protects fork integrity at protein-DNA barriers, and its absence causes checkpoint activation dependent on chromatin context. *Nucleic Acids Res* 41: 3173–3189
- Bonetti D, Rinaldi C, Vertemara J, Notaro M, Pizzul P, Tisi R, Zampella G & Longhese MP (2020) DNA binding modes influence Rap1 activity in the regulation of telomere length and MRX functions at DNA ends. *Nucleic Acids Res* 48: 2424–2441
- Bonnell E, Pasquier E & Wellinger RJ (2021) Telomere Replication: Solving Multiple End Replication Problems. *Front Cell Dev Biol* 9: 668171
- Bordelet H, Costa R, Brocas C, Dépagne J, Veaute X, Busso D, Batté A, Guérois R, Marcand S & Dubrana K (2022) Sir3 heterochromatin protein promotes non-homologous end joining by direct inhibition of Sae2. *EMBO J* 41: e108813
- Chang C-R, Wu C-S, Hom Y & Gartenberg MR (2005) Targeting of cohesin by transcriptionally silent chromatin. *Genes Dev* 19: 3031–3042
- Charifi F, Churikov D, Eckert-Boulet N, Minguet C, Jourquin F, Hardy J, Lisby M, Simon M-N & Géli V (2021) Rad52 SUMOylation functions as a molecular switch that determines a

balance between the Rad51- and Rad59-dependent survivors. *iScience* 24: 102231
- Chen M & Gartenberg MR (2014) Coordination of tRNA transcription with export at nuclear pore complexes in budding yeast. *Genes Dev* 28: 959–970
- Choudhry SK, Neal ML, Li S, Navare AT, Van Eeuwen T, Wozniak RW, Mast FD, Rout MP & Aitchison JD (2023) Nuclear pore complexes mediate subtelomeric gene silencing by regulating PCNA levels on chromatin. *J Cell Biol* 222: e202207060
- Churikov D, Charifi F, Eckert-Boulet N, Silva S, Simon M-N, Lisby M & Géli V (2016) SUMO-Dependent Relocalization of Eroded Telomeres to Nuclear Pore Complexes Controls Telomere Recombination. *Cell Rep* 15: 1242–1253
- Churikov D, Charifi F, Simon M-N & Géli V (2014) Rad59-facilitated acquisition of Y' elements by short telomeres delays the onset of senescence. *PLoS Genet* 10: e1004736
- Delamarre A, Barthe A, de la Roche Saint-André C, Luciano P, Forey R, Padioleau I, Skrzypczak M, Ginalski K, Géli V, Pasero P, *et al* (2020) MRX Increases Chromatin Accessibility at Stalled Replication Forks to Promote Nascent DNA Resection and Cohesin Loading. *Mol Cell* 77: 395-410.e3
- Dhingra N, Wei L & Zhao X (2019) Replication protein A (RPA) sumoylation positively influences the DNA damage checkpoint response in yeast. *J Biol Chem* 294: 2690–2699
- Dilworth DJ, Tackett AJ, Rogers RS, Yi EC, Christmas RH, Smith JJ, Siegel AF, Chait BT, Wozniak RW & Aitchison JD (2005) The mobile nucleoporin Nup2p and chromatin-bound Prp20p function in endogenous NPC-mediated transcriptional control. *J Cell Biol* 171: 955–965
- Douglas ME & Diffley JFX (2021) Budding yeast Rap1, but not telomeric DNA, is inhibitory for multiple stages of DNA replication in vitro. *Nucleic Acids Res* 49: 5671–5683
- Dubarry M, Loïodice I, Chen CL, Thermes C & Taddei A (2011) Tight protein-DNA interactions favor gene silencing. *Genes Dev* 25: 1365–1370
- Ebrahimi H & Donaldson AD (2008) Release of yeast telomeres from the nuclear periphery is triggered by replication and maintained by suppression of Ku-mediated anchoring. *Genes Dev* 22: 3363–3374
- Fallet E, Jolivet P, Soudet J, Lisby M, Gilson E & Teixeira MT (2014) Length-dependent processing of telomeres in the absence of telomerase. *Nucleic Acids Res* 42: 3648–3665
- Faure V, Coulon S, Hardy J & Géli V (2010) Cdc13 and telomerase bind through different mechanisms at the lagging- and leading-strand telomeres. *Mol Cell* 38: 842–852
- Förstemann K, Höss M & Lingner J (2000) Telomerase-dependent repeat divergence at the 3' ends of yeast telomeres. *Nucleic Acids Res* 28: 2690–2694
- Friedman KL, Brewer BJ & Fangman WL (1997) Replication profile of Saccharomyces cerevisiae chromosome VI. *Genes Cells Devoted Mol Cell Mech* 2: 667–678
- Fumasoni M & Murray AW (2020) The evolutionary plasticity of chromosome metabolism allows adaptation to constitutive DNA replication stress. *eLife* 9: e51963
- Gaggioli V, Lo CSY, Reverón-Gómez N, Jasencakova Z, Domenech H, Nguyen H, Sidoli S, Tvardovskiy A, Uruci S, Slotman JA, *et al* (2023) Dynamic de novo heterochromatin assembly and disassembly at replication forks ensures fork stability. *Nat Cell Biol* 25: 1017–1032
- Gasser SM & Stutz F (2023a) SUMO in the regulation of DNA repair and transcription at nuclear pores. *FEBS Lett* 597: 2833–2850
- Gasser SM & Stutz F (2023b) SUMO in the regulation of DNA repair and transcription at nuclear pores. *FEBS Lett* 597: 2833–2850
- Goto GH, Zencir S, Hirano Y, Ogi H, Ivessa A & Sugimoto K (2015) Binding of Multiple Rap1

Proteins Stimulates Chromosome Breakage Induction during DNA Replication. *PLoS Genet* 11: e1005283

- Graham IR & Chambers A (1994) Use of a selection technique to identify the diversity of binding sites for the yeast RAP1 transcription factor. *Nucleic Acids Res* 22: 124–130
- Grandin N & Charbonneau M (2007) Mrc1, a non-essential DNA replication protein, is required for telomere end protection following loss of capping by Cdc13, Yku or telomerase. *Mol Genet Genomics MGG* 277: 685–699
- Hiraga S, Robertson ED & Donaldson AD (2006) The Ctf18 RFC-like complex positions yeast telomeres but does not specify their replication time. *EMBO J* 25: 1505–1514
- Horigome C, Unozawa E, Ooki T & Kobayashi T (2019) Ribosomal RNA gene repeats associate with the nuclear pore complex for maintenance after DNA damage. *PLOS Genet* 15: e1008103
- Ivessa AS, Lenzmeier BA, Bessler JB, Goudsouzian LK, Schnakenberg SL & Zakian VA (2003) The Saccharomyces cerevisiae helicase Rrm3p facilitates replication past nonhistone protein-DNA complexes. *Mol Cell* 12: 1525–1536
- Khadaroo B, Teixeira MT, Luciano P, Eckert-Boulet N, Germann SM, Simon MN, Gallina I, Abdallah P, Gilson E, Géli V, *et al* (2009) The DNA damage response at eroded telomeres and tethering to the nuclear pore complex. *Nat Cell Biol* 11: 980–987
- Kozak ML, Chavez A, Dang W, Berger SL, Ashok A, Guo X & Johnson FB (2010) Inactivation of the Sas2 histone acetyltransferase delays senescence driven by telomere dysfunction. *EMBO J* 29: 158–170
- Kramarz K, Schirmeisen K, Boucherit V, Ait Saada A, Lovo C, Palancade B, Freudenreich C & Lambert SAE (2020) The nuclear pore primes recombination-dependent DNA synthesis at arrested forks by promoting SUMO removal. *Nat Commun* 11: 5643
- Kueng S, Oppikofer M & Gasser SM (2013) SIR proteins and the assembly of silent chromatin in budding yeast. *Annu Rev Genet* 47: 275–306
- Lapetina DL, Ptak C, Roesner UK & Wozniak RW (2017) Yeast silencing factor Sir4 and a subset of nucleoporins form a complex distinct from nuclear pore complexes. *J Cell Biol* 216: 3145–3159
- Le S, Moore JK, Haber JE & Greider CW (1999) RAD50 and RAD51 define two pathways that collaborate to maintain telomeres in the absence of telomerase. *Genetics* 152: 143–152
- Lemaître C & Soutoglou E (2014) Double strand break (DSB) repair in heterochromatin and heterochromatin proteins in DSB repair. *DNA Repair* 19: 163–168
- Lieb JD, Liu X, Botstein D & Brown PO (2001) Promoter-specific binding of Rap1 revealed by genome-wide maps of protein-DNA association. *Nat Genet* 28: 327–334
- Litwin I, Bakowski T, Szakal B, Pilarczyk E, Maciaszczyk-Dziubinska E, Branzei D & Wysocki R (2018) Error-free DNA damage tolerance pathway is facilitated by the Irc5 translocase through cohesin. *EMBO J* 37: e98732
- Liu HW, Bouchoux C, Panarotto M, Kakui Y, Patel H & Uhlmann F (2020) Division of Labor between PCNA Loaders in DNA Replication and Sister Chromatid Cohesion Establishment. *Mol Cell* 78: 725-738.e4
- Makovets S, Herskowitz I & Blackburn EH (2004) Anatomy and dynamics of DNA replication fork movement in yeast telomeric regions. *Mol Cell Biol* 24: 4019–4031
- Marcomini I, Shimada K, Delgoshaie N, Yamamoto I, Seeber A, Cheblal A, Horigome C, Naumann U & Gasser SM (2018) Asymmetric Processing of DNA Ends at a Double-Strand Break Leads to Unconstrained Dynamics and Ectopic Translocation. *Cell Rep* 24: 2614-

2628.e4
- Martin H, Doumic M, Teixeira MT & Xu Z (2021) Telomere shortening causes distinct cell division regimes during replicative senescence in Saccharomyces cerevisiae. *Cell Biosci* 11: 180
- Meister P, Gehlen LR, Varela E, Kalck V & Gasser SM (2010) Visualizing Yeast Chromosomes and Nuclear Architecture. In *Methods in Enzymology* pp 535–567. Elsevier
- Mills KD, Sinclair DA & Guarente L (1999) MEC1-dependent redistribution of the Sir3 silencing protein from telomeres to DNA double-strand breaks. *Cell* 97: 609–620
- Nagai S, Dubrana K, Tsai-Pflugfelder M, Davidson MB, Roberts TM, Brown GW, Varela E, Hediger F, Gasser SM & Krogan NJ (2008) Functional targeting of DNA damage to a nuclear pore-associated SUMO-dependent ubiquitin ligase. *Science* 322: 597–602
- Negrini S, Ribaud V, Bianchi A & Shore D (2007) DNA breaks are masked by multiple Rap1 binding in yeast: implications for telomere capping and telomerase regulation. *Genes Dev* 21: 292–302
- Nikolov I & Taddei A (2016) Linking replication stress with heterochromatin formation. *Chromosoma* 125: 523–533
- Penzo A, Dubarry M, Brocas C, Zheng M, Mangione RM, Rougemaille M, Goncalves C, Lautier O, Libri D, Simon M-N, *et al* (2023) A R-loop sensing pathway mediates the relocation of transcribed genes to nuclear pore complexes. *Nat Commun* 14: 5606
- Pinzaru AM, Kareh M, Lamm N, Lazzerini-Denchi E, Cesare AJ & Sfeir A (2020) Replication stress conferred by POT1 dysfunction promotes telomere relocalization to the nuclear pore. *Genes Dev* 34: 1619–1636
- Psakhye I & Jentsch S (2012) Protein group modification and synergy in the SUMO pathway as exemplified in DNA repair. *Cell* 151: 807–820
- Psakhye I, Kawasumi R, Abe T, Hirota K & Branzei D (2023) PCNA recruits cohesin loader Scc2 to ensure sister chromatid cohesion. *Nat Struct Mol Biol* 30: 1286–1294
- Ptak C & Wozniak RW (2016) Nucleoporins and chromatin metabolism. *Curr Opin Cell Biol* 40: 153–160
- Rivard RS, Chang Y-C, Ragland RL, Thu Y-M, Kassab M, Mandal RS, Van Riper SK, Kulej K, Higgins L, Markowski TM, *et al* (2024) Improved detection of DNA replication fork-associated proteins. *Cell Rep* 43: 114178
- Sacher M, Pfander B, Hoege C & Jentsch S (2006) Control of Rad52 recombination activity by double-strand break-induced SUMO modification. *Nat Cell Biol* 8: 1284–1290
- Sakuma S & D'Angelo MA (2017) The roles of the nuclear pore complex in cellular dysfunction, aging and disease. *Semin Cell Dev Biol* 68: 72–84
- Schirmeisen K, Naiman K, Fréon K, Besse L, Chakraborty S, Saada AA, Carr AM, Kramarz K & Lambert SAE (2024) SUMO protease and proteasome recruitment at the nuclear periphery differently affect replication dynamics at arrested forks. *Nucleic Acids Res*: gkae526
- Schmid M, Durussel T & Laemmli UK (2004) ChIC and ChEC; genomic mapping of chromatin proteins. *Mol Cell* 16: 147–157
- Simon M-N, Churikov D & Géli V (2016) Replication stress as a source of telomere recombination during replicative senescence in Saccharomyces cerevisiae. *FEMS Yeast Res* 16: fow085
- Simon M-N, Dubrana K & Palancade B (2024) On the edge: how nuclear pore complexes rule genome stability. *Curr Opin Genet Dev* 84: 102150
- Sinha M, Watanabe S, Johnson A, Moazed D & Peterson CL (2009) Recombinational repair

within heterochromatin requires ATP-dependent chromatin remodeling. *Cell* 138: 1109–1121

- Srinivasan M, Fumasoni M, Petela NJ, Murray A & Nasmyth KA (2020) Cohesion is established during DNA replication utilising chromosome associated cohesin rings as well as those loaded de novo onto nascent DNAs. *eLife* 9: e56611
- Stivison EA, Young KJ & Symington LS (2020) Interstitial telomere sequences disrupt break-induced replication and drive formation of ectopic telomeres. *Nucleic Acids Res* 48: 12697–12710
- Strecker J, Stinus S, Caballero MP, Szilard RK, Chang M & Durocher D (2017) A sharp Pif1-dependent threshold separates DNA double-strand breaks from critically short telomeres. *eLife* 6: e23783
- Su XA, Dion V, Gasser SM & Freudenreich CH (2015) Regulation of recombination at yeast nuclear pores controls repair and triplet repeat stability. *Genes Dev* 29: 1006–1017
- Sundararajan R, Gellon L, Zunder RM & Freudenreich CH (2010) Double-strand break repair pathways protect against CAG/CTG repeat expansions, contractions and repeat-mediated chromosomal fragility in Saccharomyces cerevisiae. *Genetics* 184: 65–77
- Taddei A, Hediger F, Neumann FR, Bauer C & Gasser SM (2004) Separation of silencing from perinuclear anchoring functions in yeast Ku80, Sir4 and Esc1 proteins. *EMBO J* 23: 1301–1312
- Taddei A, Schober H & Gasser SM (2010) The budding yeast nucleus. *Cold Spring Harb Perspect Biol* 2: a000612
- Teixeira MT (2013) Saccharomyces cerevisiae as a Model to Study Replicative Senescence Triggered by Telomere Shortening. *Front Oncol* 3: 101
- Teixeira-Silva A, Ait Saada A, Hardy J, Iraqui I, Nocente MC, Fréon K & Lambert SAE (2017) The end-joining factor Ku acts in the end-resection of double strand break-free arrested replication forks. *Nat Commun* 8: 1982
- Therizols P, Fairhead C, Cabal GG, Genovesio A, Olivo-Marin J-C, Dujon B & Fabre E (2006) Telomere tethering at the nuclear periphery is essential for efficient DNA double strand break repair in subtelomeric region. *J Cell Biol* 172: 189–199
- Tittel-Elmer M, Alabert C, Pasero P & Cobb JA (2009) The MRX complex stabilizes the replisome independently of the S phase checkpoint during replication stress. *EMBO J* 28: 1142–1156
- Tye S, Ronson GE & Morris JR (2021) A fork in the road: Where homologous recombination and stalled replication fork protection part ways. *Semin Cell Dev Biol* 113: 14–26
- Van de Vosse DW, Wan Y, Lapetina DL, Chen W-M, Chiang J-H, Aitchison JD & Wozniak RW (2013) A role for the nucleoporin Nup170p in chromatin structure and gene silencing. *Cell* 152: 969–983
- Whalen JM, Dhingra N, Wei L, Zhao X & Freudenreich CH (2020) Relocation of Collapsed Forks to the Nuclear Pore Complex Depends on Sumoylation of DNA Repair Proteins and Permits Rad51 Association. *Cell Rep* 31: 107635
- Zentner GE, Kasinathan S, Xin B, Rohs R & Henikoff S (2015) ChEC-seq kinetics discriminates transcription factor binding sites by DNA sequence and shape in vivo. *Nat Commun* 6: 8733
- Zhao X & Blobel G (2005) A SUMO ligase is part of a nuclear multiprotein complex that affects DNA repair and chromosomal organization. *Proc Natl Acad Sci U S A* 102: 4777–4782

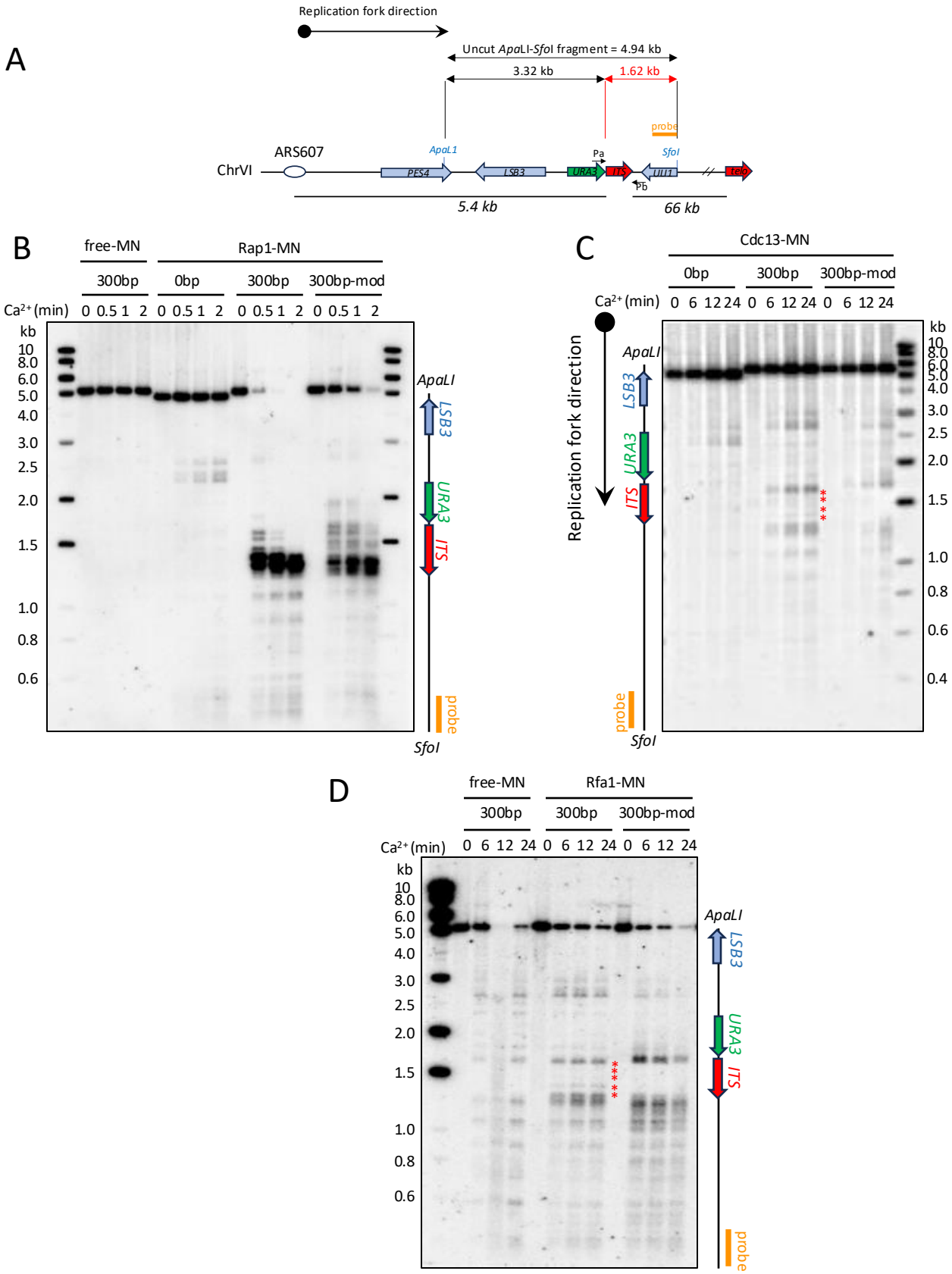

Figure 1 : Replication stress at the interstitial telomeric sequence is dependent on the tight binding of Rap1. (A) Schematic of ITS at ARS607. A DNA fragment containing 0bp or 300 bp of TG_{1-3} telomeric sequence (ITS) or 300bp of TG_{1-2} sequence (ITS-mod) and the *URA3* gene was introduced at 5.4kb of the early origin ARS607, replacing a locus containing *HIS2* and a tRNA(Ala) gene. The schematic shows the structure of the 4,94kb *ApaL1-SfoI* restriction fragment. The position of the probe used to analyze cleavage by ChEC is shown. **(B)** *In vivo* ChEC with Rap1- and free-MN. Genomic DNA was extracted after increasing incubation time with Ca^{2+}, digested with *ApaL1-SfoI* and analyzed by Southern blot with the radiolabelled probe indicated in the figure. The position of the ITS is depicted on the right. Free-MN is fused to a NLS and expressed from the *REB1* promoter. **(C)** *In vivo* ChEC with Cdc13- and free-MN. **(D)** *In vivo* ChEC with Rfa1- and free-MN.

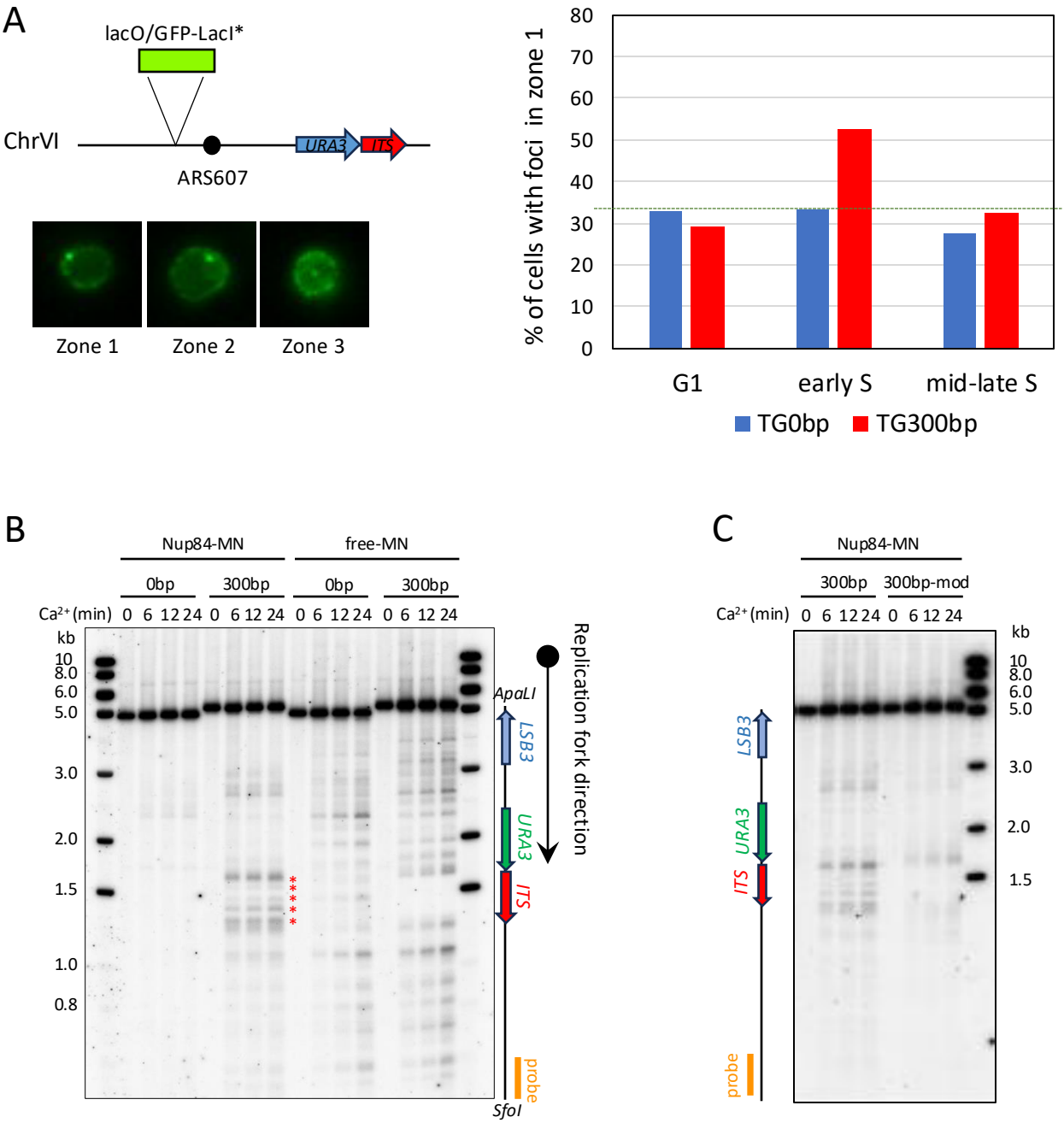

Figure 2: Interstitial telomeric sequences relocalize to the NPCs. (A) The ITS locus was visualized by binding of lacI*-GFP to a LacO array introduced 6,4 kb from the ITS. LacI*-GFP binding is not a barrier to replication fork progression (Dubarry et al., 2011). The nuclear periphery was marked by GFP-Nup49. The position of the LacI*-GFP signal was scored into one of the three zones of equal-area in cells in G1 (no bud), early S (tiny buds) and mid/late S phase (small to large buds) (see also Figure S4). At least one hundred cells from 3 independent clones were monitored in each category. **(B)** *In vivo* ChEC with Nup84- and free-MN. Genomic DNA was extracted after increasing incubation time with Ca^{2+}, digested with *ApaL1-SfoI* and analyzed by Southern blot with the radiolabelled probe indicated in the figure. The position of the ITS is schematized on right. **(C)** Comparison of the cleavage by Nup84-MN ChEC of the loci containing the ITS (noted 300bp) and the ITS-mod (noted 300bpmod).

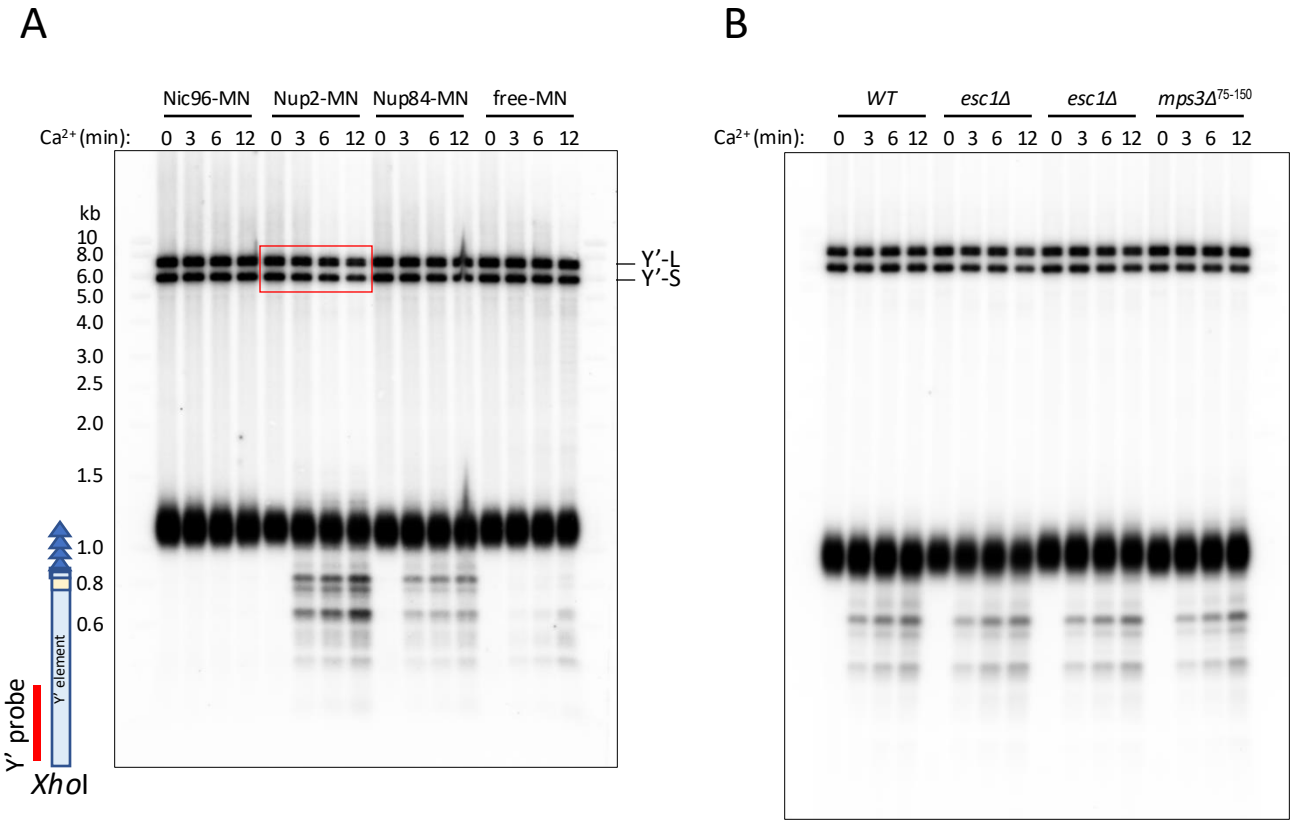

Figure 3: Interaction of natural telomeres with the NPCS. (A) *In vivo* ChEC with MN fused to different nucleoporins. Southern blot analysis of the cleavage with the indicated fusion proteins revealed with a Y' radiolabelled probe. Genomic DNA was digested with *XhoI.* The position of the telomeric and subtelomeric sequences is schematized on the left. The cleavage pattern is compared with that of cells expressing a MN-NLS fusion from the *REB1* promoter (free-MN) as a control. The red square shows specific Nup2-MN cleavage of the internal Y' subtelomeric repeats. **(B)** *In vivo* ChEC with Nup84-MN in clones of the indicated genotypes. The Southern blot was probed as in (A).

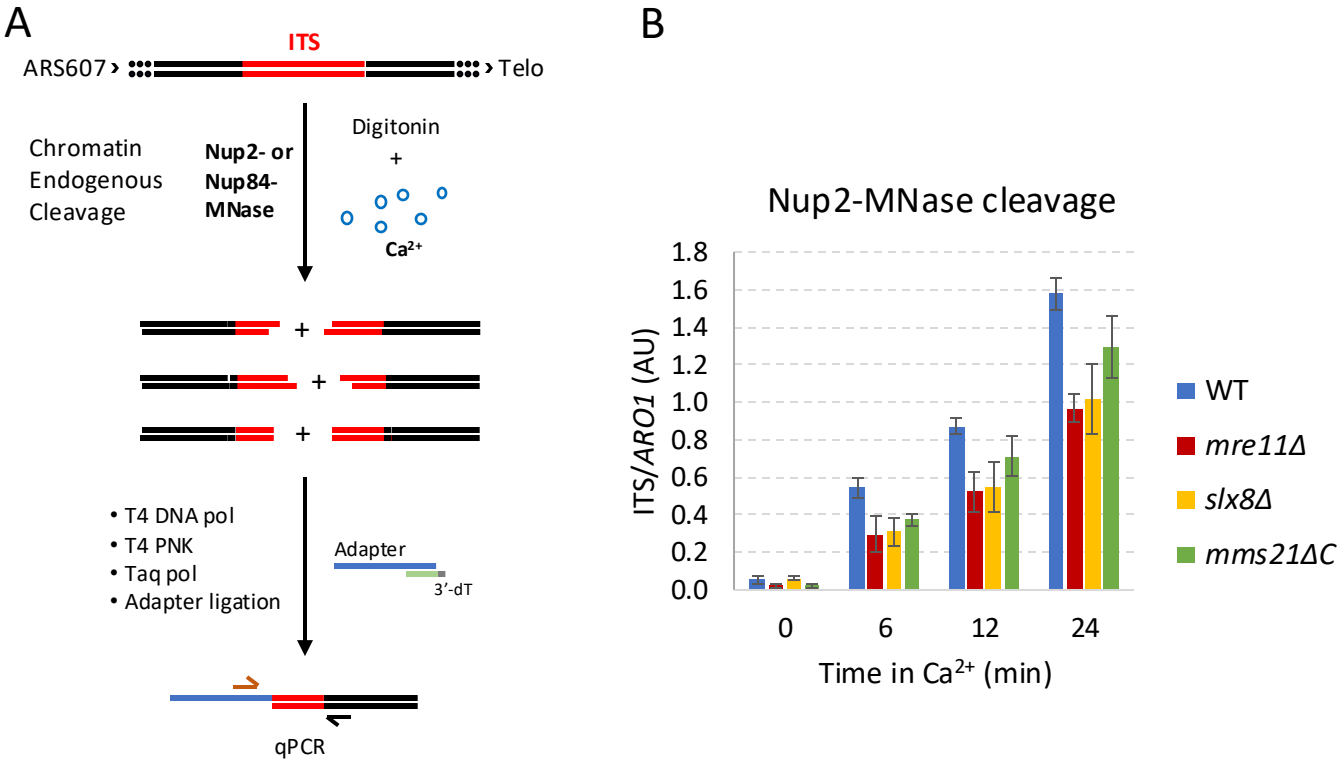

Figure 4: Mre11 and the SUMO pathway are involved in the relocalization of the ITS to NPCs. **(A)** Schematic of the ChEC-qPCR. The enzymatic treatment steps required to prepare DNA digested with MNase for ligation with a qPCR adaptor are shown. The annealing positions of the adaptor-specific and genomic primers are indicated. **(B)** Quantification of the ITS cleavage with Nup2-MNase at different times of Ca^{2+} incubation in *WT* and mutant cells of the indicated genotypes. qPCR efficiencies of the ITS cleavage products were normalized by the level of *ARO1* locus amplification. Two-way ANOVA test *p*-values are as follows: WT (n=12) versus *mre11*Δ (n=6) $p = 6.63 \times 10^{-8}$, versus *slx8*Δ (n=3) $p = 5.07 \times 10^{-5}$, versus *mms21*ΔC (n=5) $p = 0.005$.

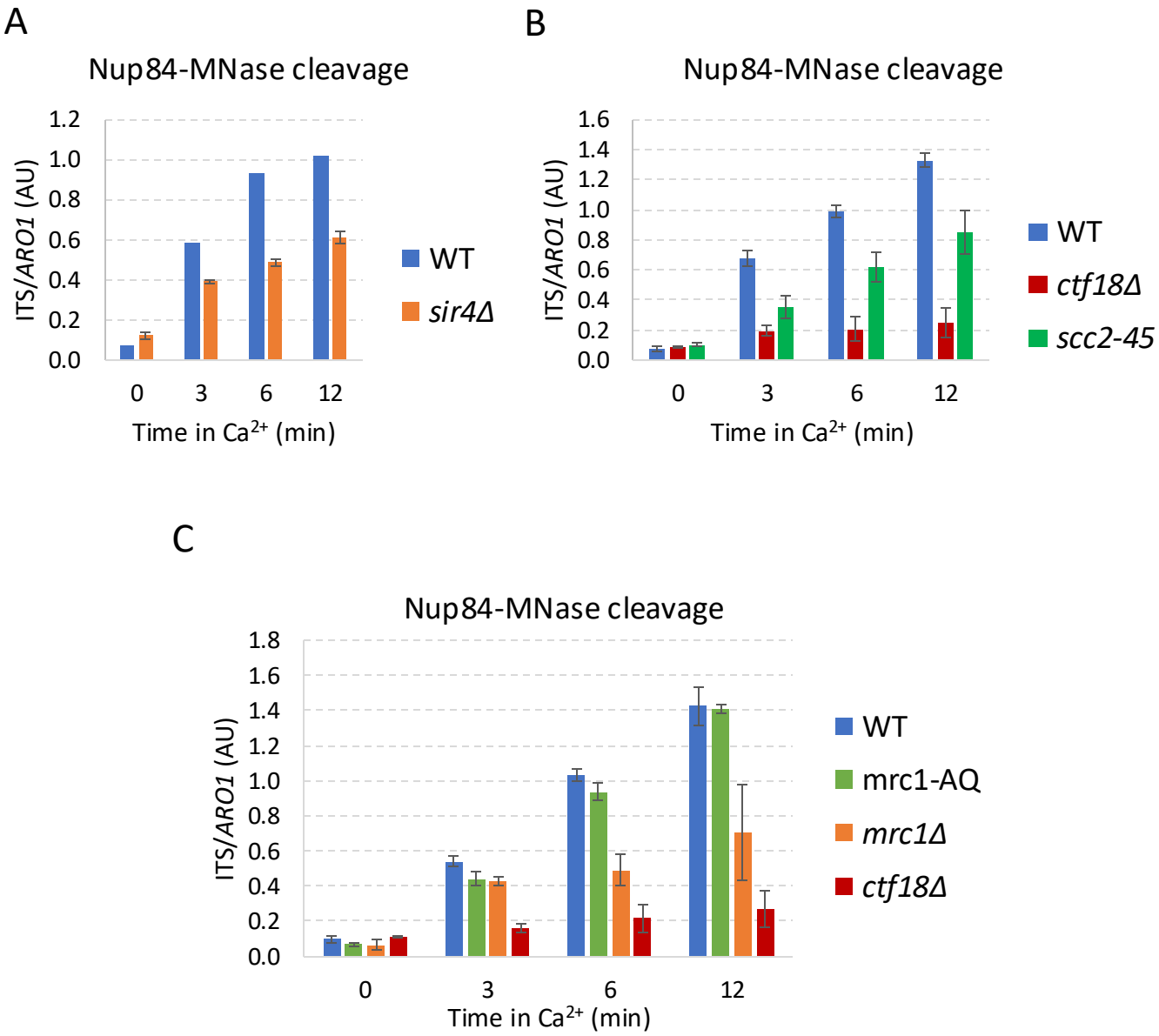

Figure 5: Sir4 and Ctf18-facilitated SCC cohesion but not the S-phase checkpoint are required for relocalization to NPCs. (A) Quantification of the ITS cleavage by Nup84-MNase at increasing incubation times with Ca^{2+} in *WT* and *sir4Δ* cells. qPCR efficiencies of the ITS cleavage products were normalized by the level of *ARO1* locus amplification. Two-way ANOVA test p-value equals 9.23×10^{-6} for WT (n=1) versus *sir4*Δ (n=3). **(B)** Quantification of the ITS cleavage by Nup84-MNase at increasing incubation time with Ca^{2+} in WT, *ctf18Δ* and *scc2-45* cells. scc2-45 were grown at 25°C and shifted to semi-permissive temperature (30°C) for 1 hour. qPCR efficiencies of the ITS cleavage products were normalized by the level of *ARO1* locus amplification. Two-way ANOVA test *p*-values: WT (n=5) versus *ctf18*Δ (n=2) $p = 7.10 \times 10^{-11}$, WT versus *scc2-45* (n=5) $p = 5.50 \times 10^{-6}$. **(C)** Quantification of the ITS cleavage by Nup84-MNase at increasing incubation time with Ca^{2+} in *WT* and mutant cells of the indicated genotypes. The *ctf18Δ* data are the same as in (B) and are shown for comparison. qPCR efficiencies of the ITS cleavage products were normalized by the level of *ARO1* locus amplification. Two-way ANOVA test *p*-values are as follows: WT (n=5) versus *mrc1-AQ* (n=3) $p = 0.221$, versus *mrc1*Δ (n=2) $p = 6.38 \times 10^{-5}$.

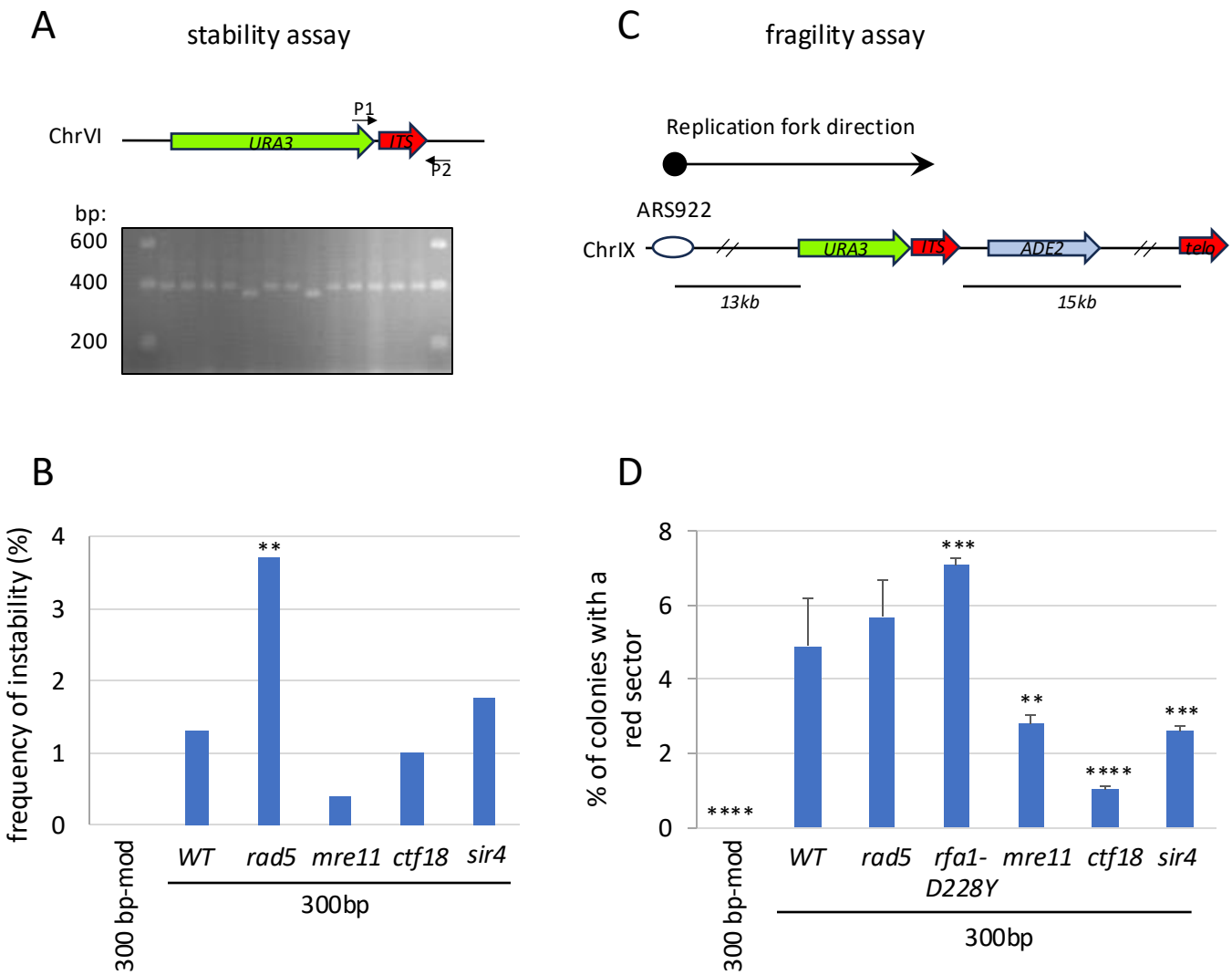

Figure 6: Tight binding of Rap1 to ITS induces instability and fragility. (A) *Instability assay*. Individual colonies were analyzed for ITS length by PCR using indicated primers. PCR length was monitored by 2% agarose electrophoresis. **(B)** Instability was measured as the percent of colonies that showed either expansion or retraction of the ITS. Measurement are from at least two individually isolated clones for each genotype. WT: n=602, *rad5*: n=395, *mre11*: n=449, TG300mut: n=244, *ctf18*: n=284, *sir4*: n=284. (**) P<0.01 compared with wild type with Dunnett's multiple comparison post-Anova test. **(C)** *Fragility assay*. Schematic of the ITS integrated 13 kb away from ARS922. The strain carries a complete deletion of *ADE2* at its natural locus. The *ADE2* gene was introduced downstream of the ITS in order to visualize the loss of the terminal fragment as red cells. **(D)** Fragility was measured as the percentage of colonies with at least one red sector. A fraction of the red colonies was tested for terminal fragment loss by PCR and telo-PCR (see Materials and methods and figure S8B). Measurements are from at least three individually isolated clones per genotype. At least 1000 colonies were analyzed for each phenotype. (**) P<0.01 (***), P<0.001, (****) P<0.0001 compared with wild type with Dunnett's multiple comparison post-Anova test.

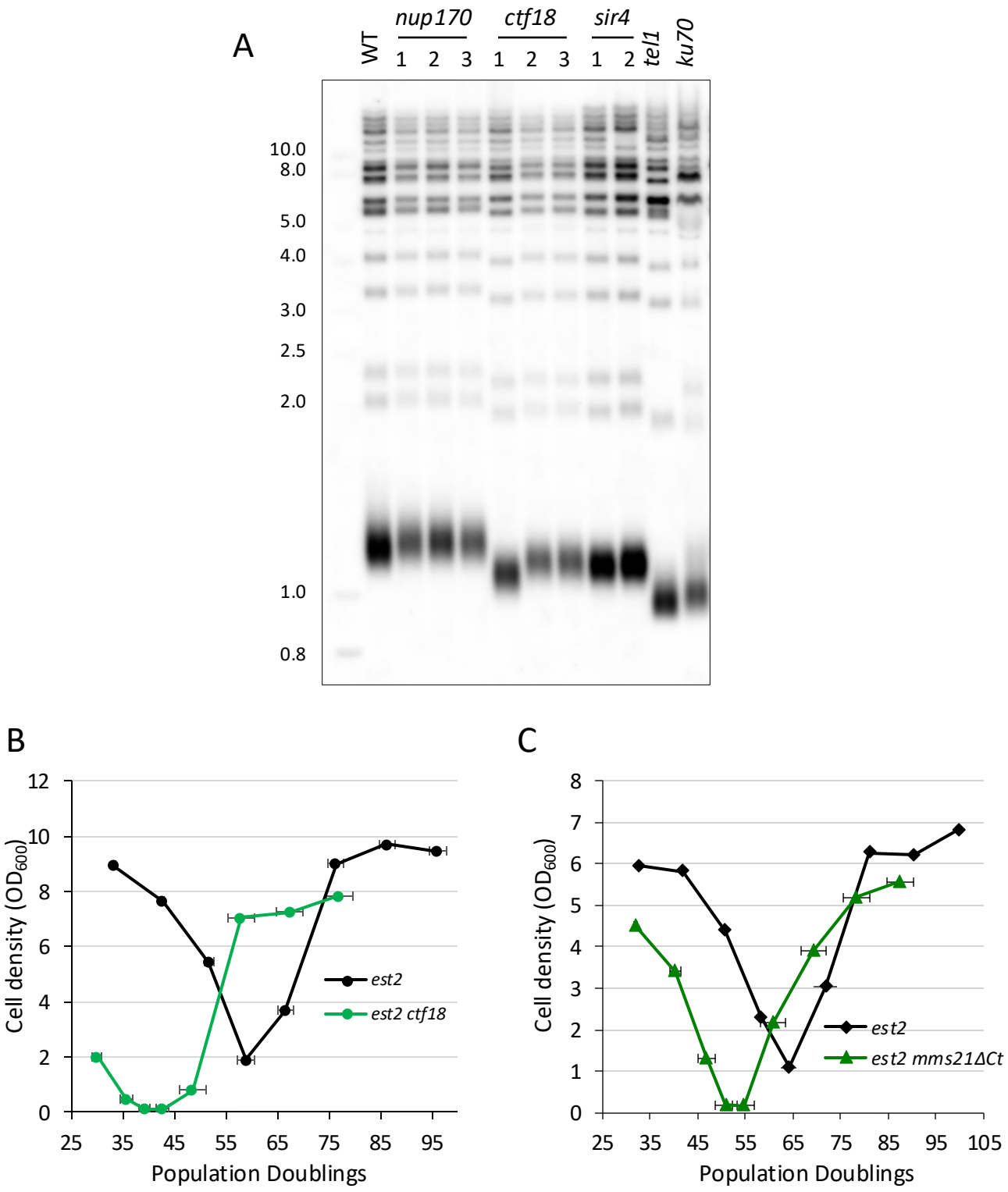

Figure 7: Inactivation of *CTF18* and *MMS21* accelerates senescence. A) *short telomeres in ctf18 and sir4 mutants*. Telomere length was analyzed by TG1-3 probed Southern blot analysis of XhoI-digested DNA isolated from independent clones of the indicated genotypes. **B)** *ctf18 accelerates senescence in the absence of telomerase*. Mean replicative senescence curves of *est2* (n=9) and *est2Δ ctf18* (n = 10). Each clone issued from a spore colony was propagated in liquid culture through daily serial dilution. OD600 was measured every day to estimate the cell density reached in 24 h. PD numbers were estimated from the initial spores. Error bars are SDs. **B)** *mms21ΔCt accelerates senescence*. Mean replicative senescence curves of *est2* (n=3) and *est2Δ mms21ΔCt* (n = 8). Error bars are SDs.

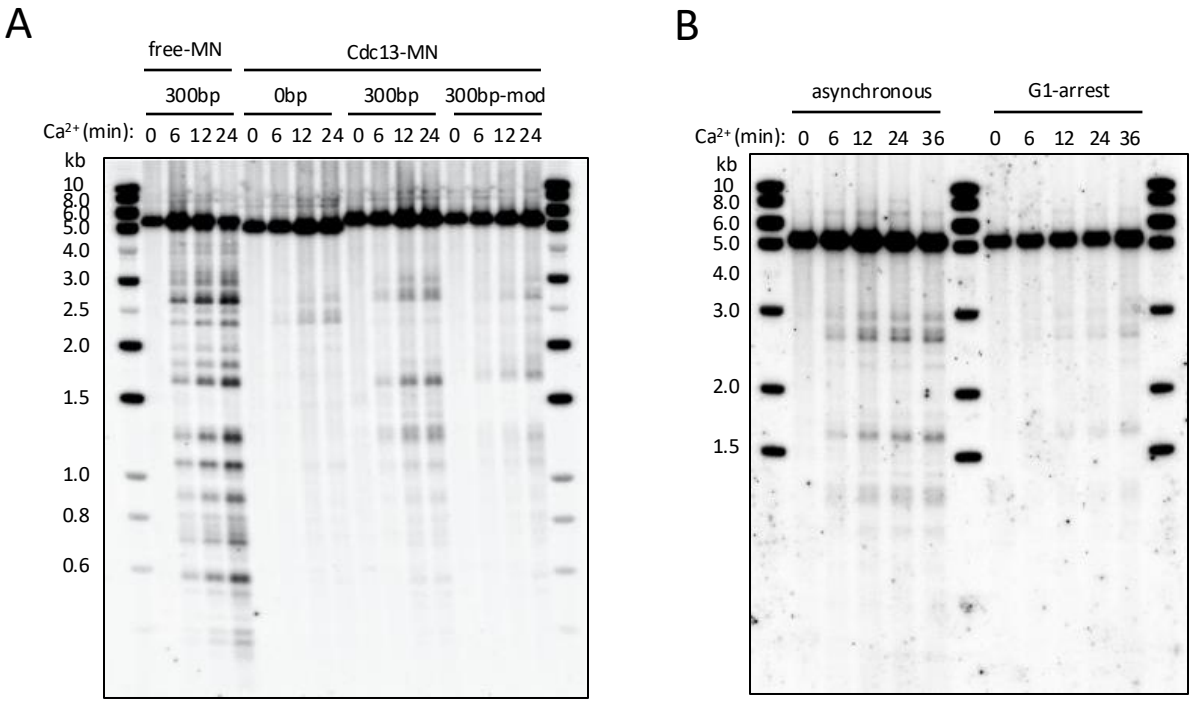

Supplementary Figure 1: ***In vivo*** **ChEC with Cdc13- and free-MN. (A)** Duplicate with independently isolated clones of the ChEC analysis shown in Figure 1C. **(B)** Interstitial telomeric sequences are resistant to Cdc13-MN cleavage in G1 cells. Cells in the right panel were arrested for 90 minutes with α-factor prior to permeabilization and incubation with Ca^{2+} for the indicated times and compared with cells from an asynchronous culture (left panel). α-factor were added in all buffers of the ChEC assay to prevent G1 exit during incubations.

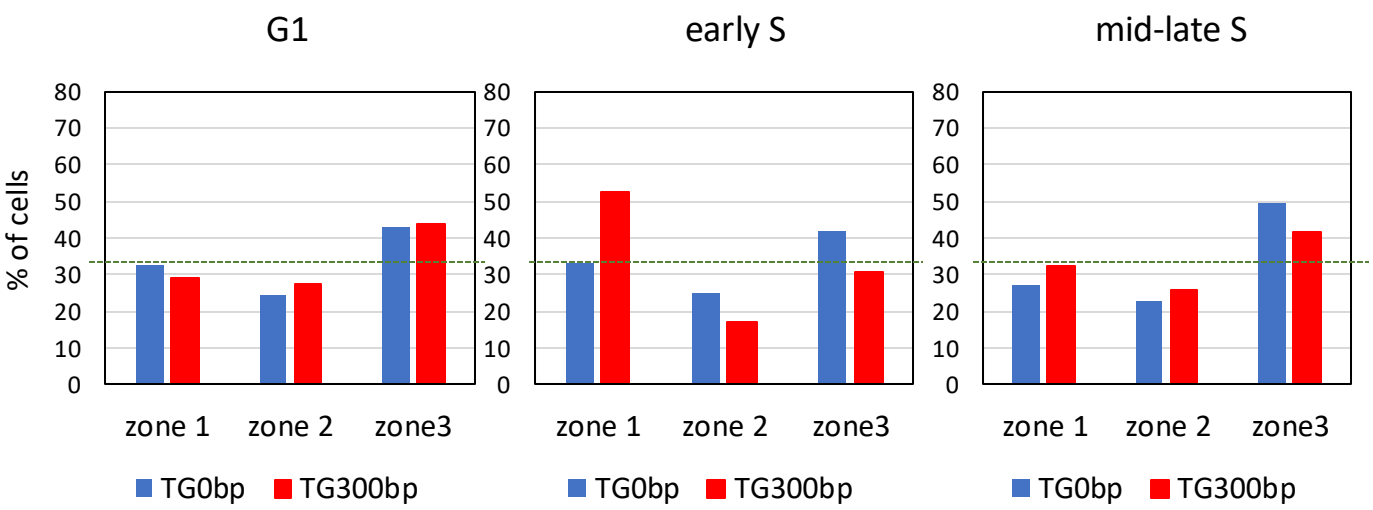

Supplementary Figure 2: Repartition of the LacI*-GFP foci into three equal areas of the nucleus marked by GFP-Nup49. Cells from asynchronous cultures were classified as G1 (no bud), early S (tiny buds) and mid/late S (medium to large buds with a nucleus at the center of the mother cell). n=107 (TG0bp/G1), n= 96 (TG0bp early S), n=135 (TG0bp, mid-late S), n=124 (TG300bp, G1), n=95 (TG300bp, early S), n=132 (TG300bp, mid-late S) from two independent clones for each genotype.

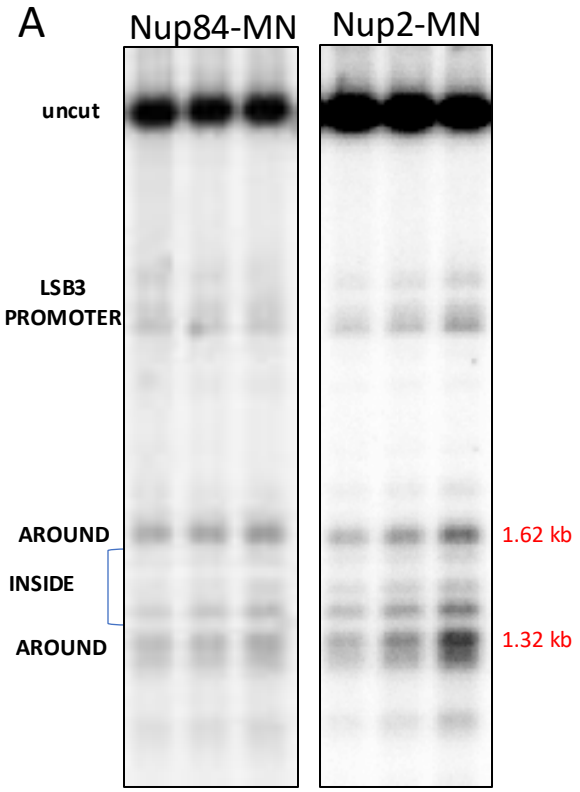

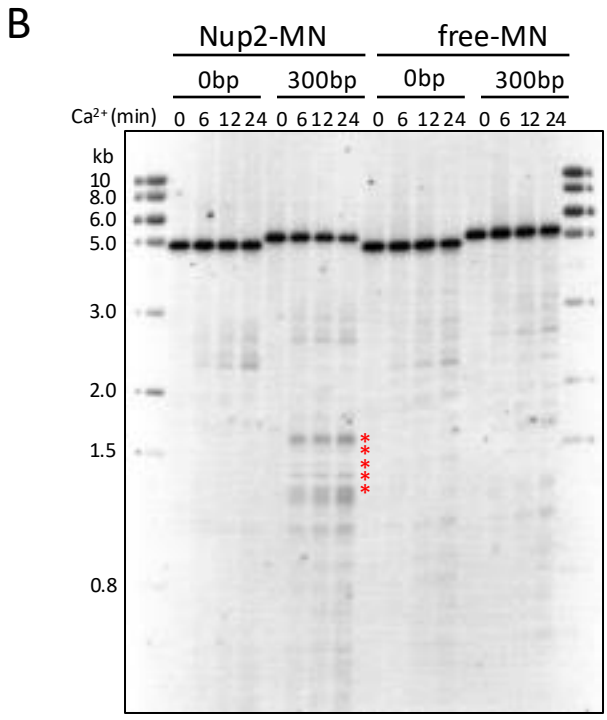

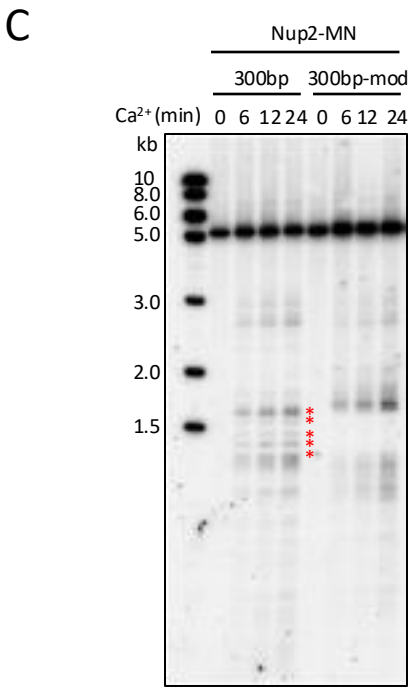

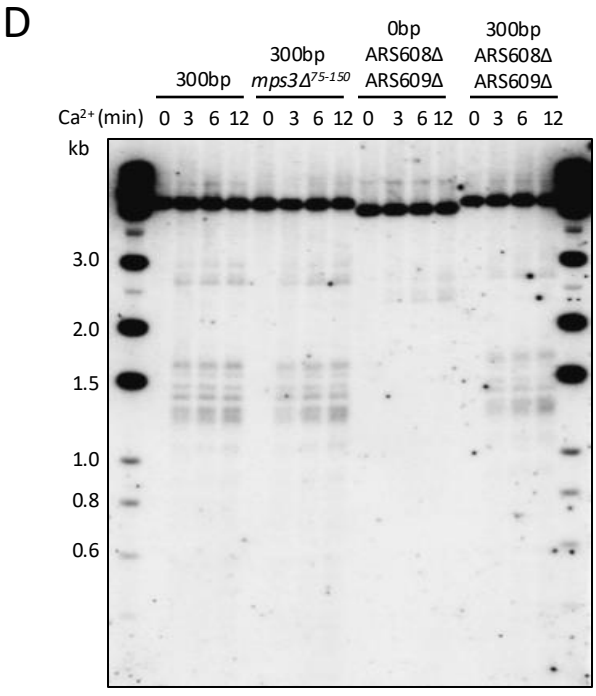

Supplementary Figure 3: In vivo ChEC with Nup2-MN. **(A)** comparison of the cleavage profiles with Nup84-MN (left panel) and Nup2-MN (right). The position of the cleavage sites relative to the ITS are defined according to the map of the fragment. **(B)** Comparison of in vivo Nup2 and free-MN ChEC products. Nup2-MN specific cleavages are marked by red stars. **(C)** Comparison of in vivo Nup2-MN ChEC cleavage products in cells carrying ITS (300bp) and ITS-mod (300bp-mod). **(D)** Comparison of in vivo Nup2 and free-MN ChEC products in cells of the indicated genotype.

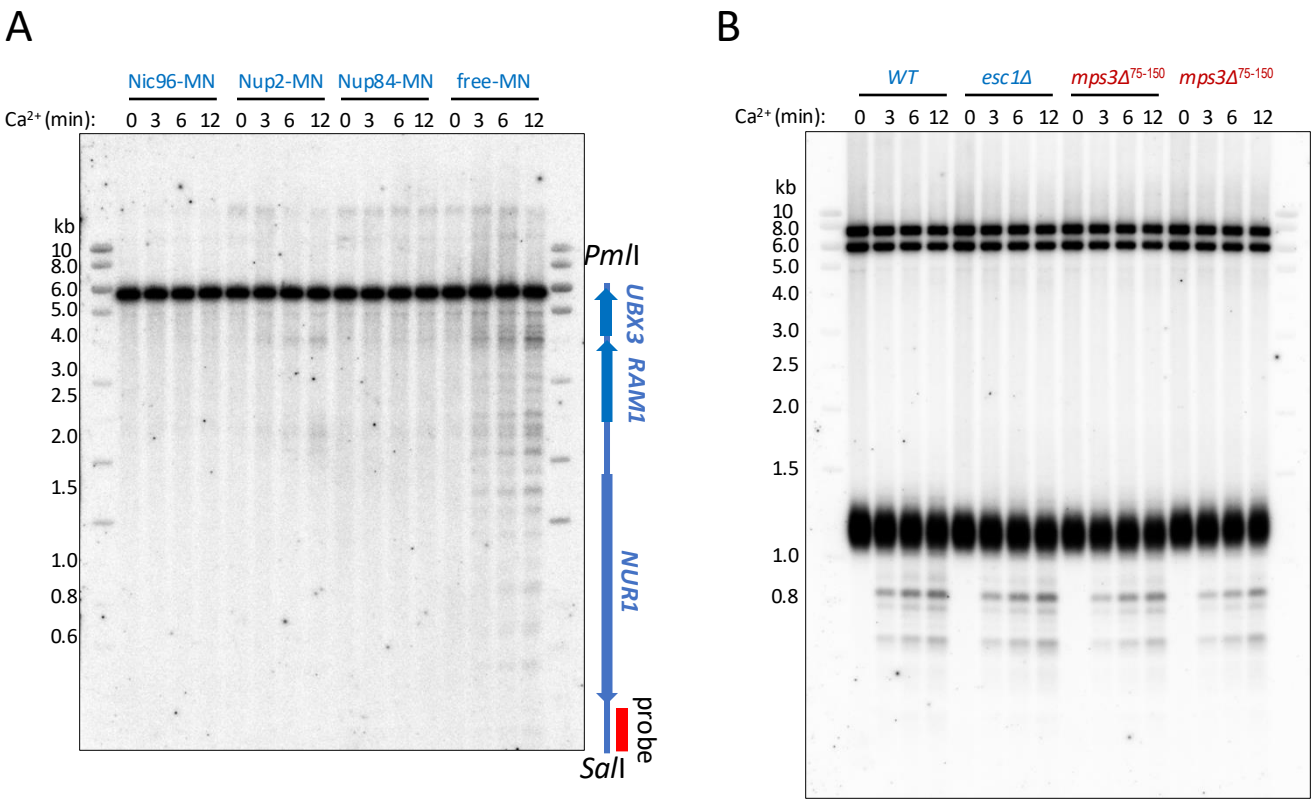

Supplementary Figure 4: Interaction of natural telomeres with the NPCS. (A) The DNA samples used in Figure 2A were digested with *SalI* and *PmlI*. The southern blot was hybridized with a radiolabelled probe hybridizing to a 5,8 kb portion of the genome with no known barrier to replication fork progression (schematized on the right). **(C)** *In vivo* ChEC with Nup84-MN in clones of the indicated genotypes. Southern blot analysis of the cleavage revealed with a Y' radiolabelled probe.

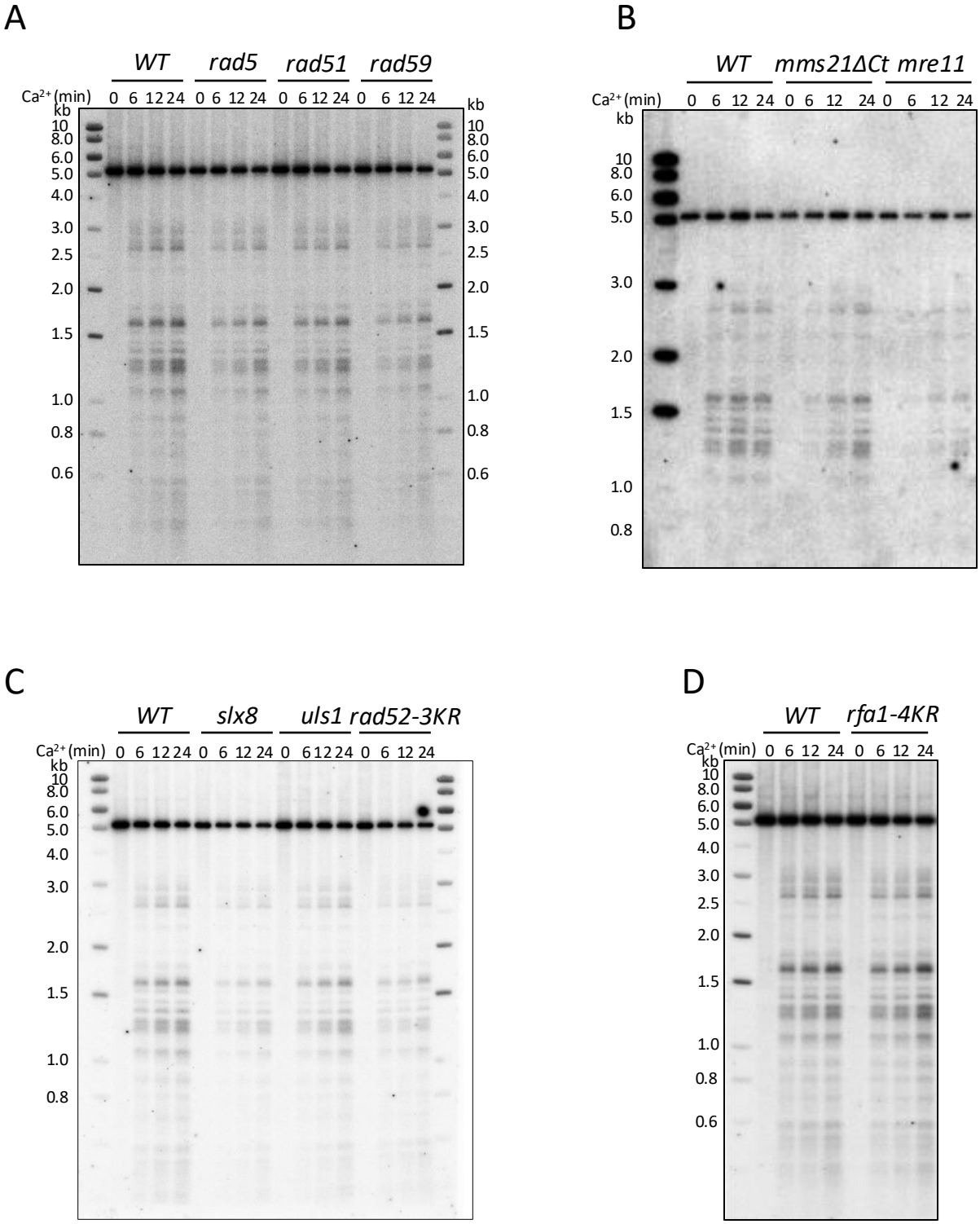

Supplementary Figure 5: Resection and SUMOylation, but not recombination, are important factors of the relocalization to NPCs. (A-D) Southern blot analysis of *in vivo* Nup2-MN ChEC cleavage products in WT and mutants of the indicated genotypes.

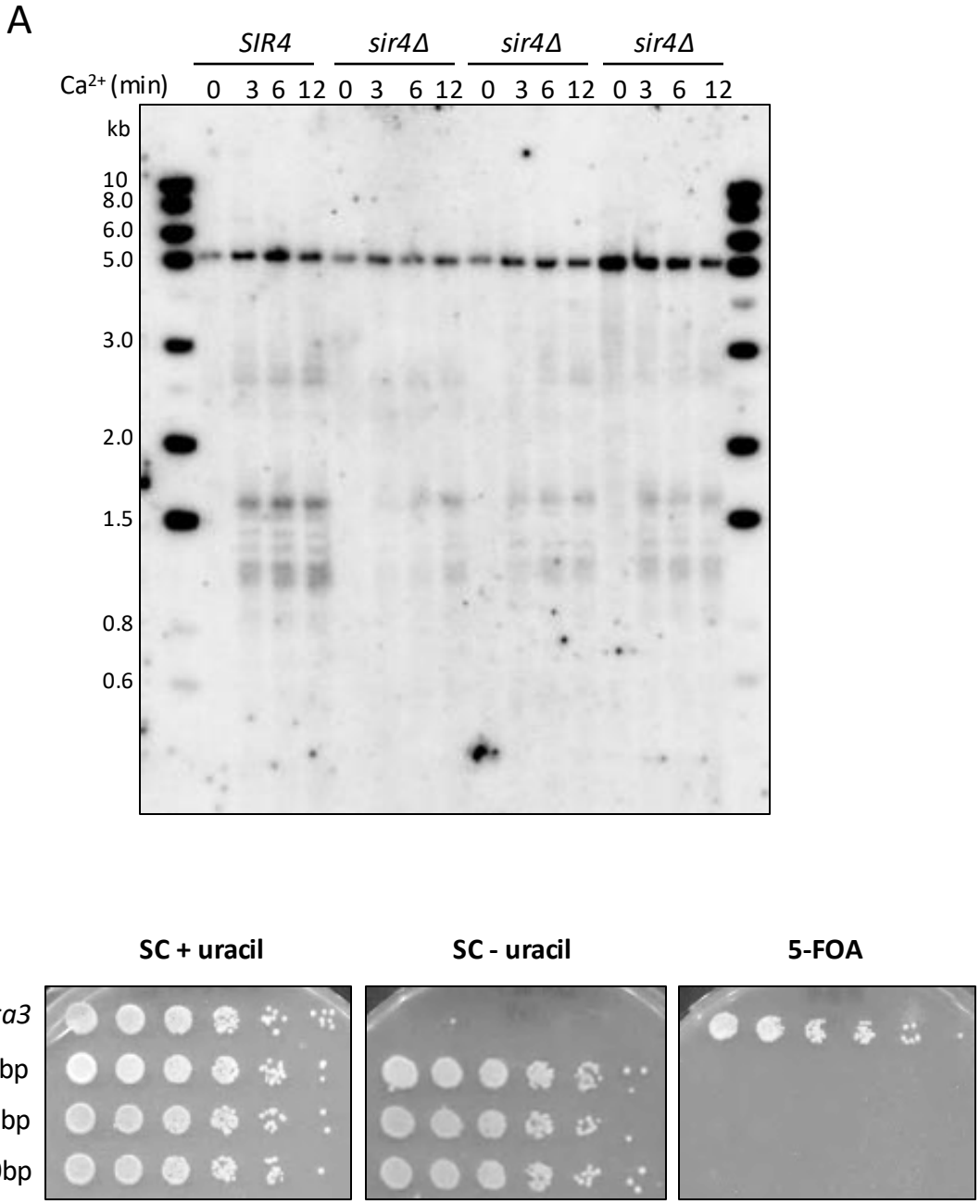

Supplementary Figure 6: Sir4 is required for the contact between ITS and NPCs. (A) Southern blot analysis of *in vivo* Nup2-MN ChEC cleavage products in WT and *sir4Δ* cells. The three *sir4Δ* panels correspond to three independent clones. **(B)** The interstitial telomeric sequence did not silenced the flanked *URA3* gene. Increasing length of ITS did not affect the growth rate in the absence of uracil nor permitted the growth on plates containing 5-Fluoroorotic acid, a poison for *URA3* expressing cells.

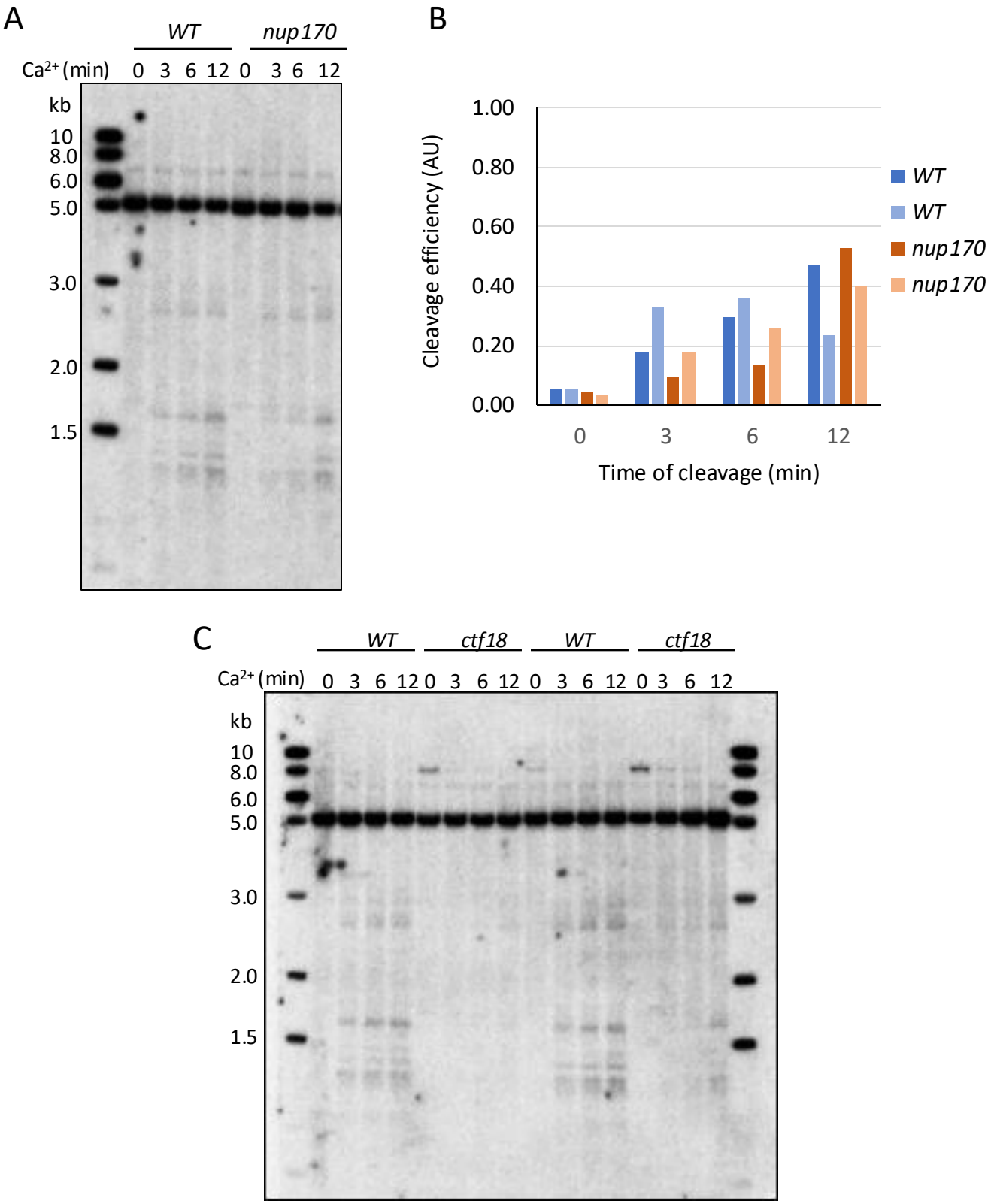

Supplementary Figure 7: Ctf18 is required for anchoring to NPCs. (A) Southern blot analysis of *in vivo* Nup84-MNase ChEC cleavage products in WT and *nup170* cells. **(B)** Quantification of Nup84-MNase cleavage products at different times of Ca^{2+} incubation in two independent *WT* and *nup170Δ* clones. qPCR efficiencies were normalized with qPCR at an *ARO1* locus. **(C)** Southern blot analysis of in vivo Nup84-MNase ChEC cleavage products in WT and *ctf18Δ* cells. The two *ctf18Δ* panels correspond to independent clones.

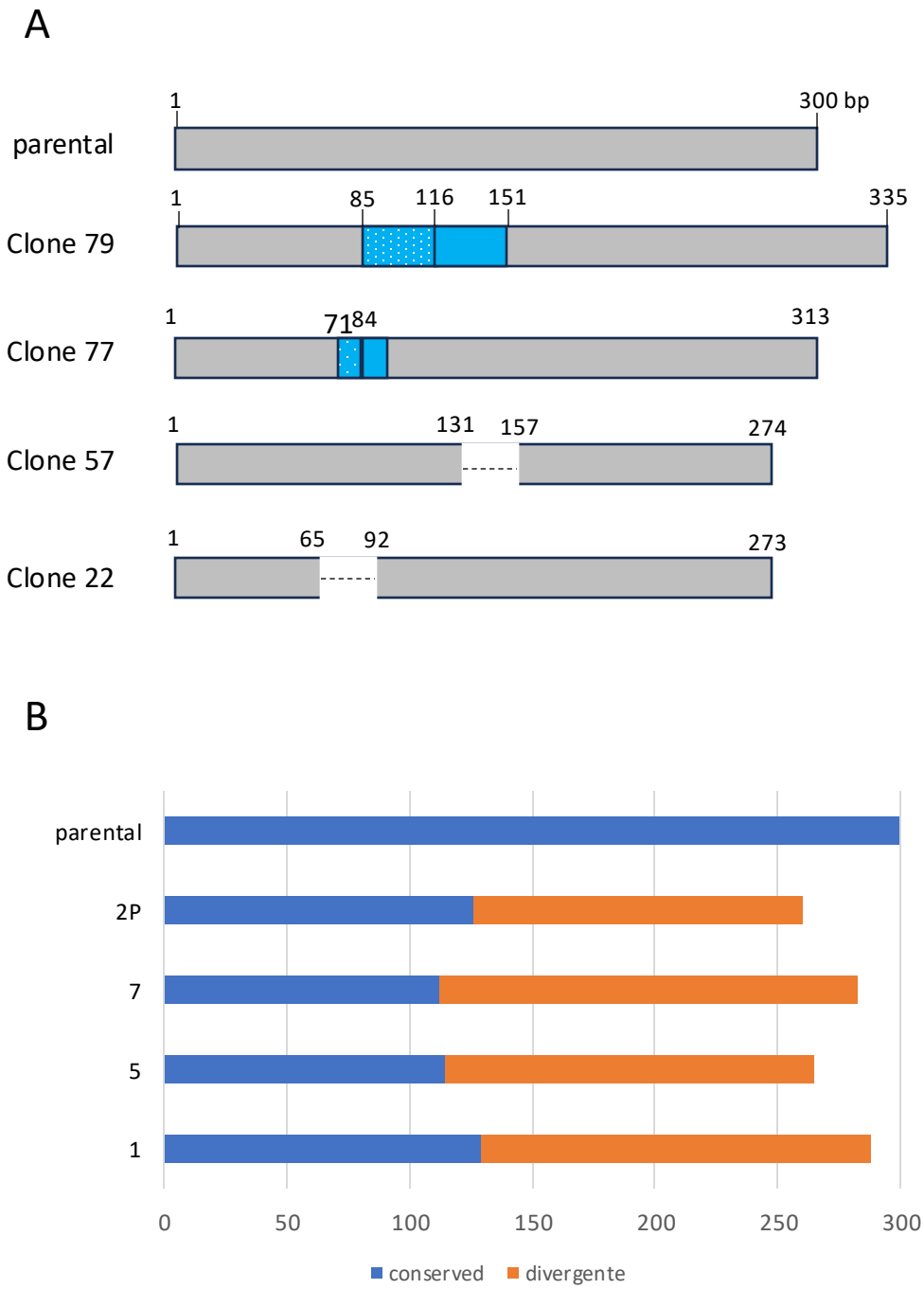

Supplementary Figure 8: ITS confers instability and fragility. **(A)** WT cells showing either expansion or contraction of the ITS were sequenced after ITS amplification by PCR. Compared to the original sequence, expansion corresponded to short duplications within the ITS (blue boxes). Contraction corresponded to short deletions within the ITS (dashed lines). Both occurred in the first half of the ITS sequence. **(B)** red colonies from the fragility assay were submitted to TeloPCR with appropriate primers to amplify *de novo* telomere at the ITS. Sequences of the PCR fragment were aligned to the parental ITS sequence. The blue to orange transition marks the point of divergence with the parental sequence and the orange the length of the added *de novo* telomeres.

Supplementary table 1: strains used in this study

Strain name	Genotype	Origin
W1588	*MATα ade2-1 can1-100 his3-11,15 leu2-3-112 trp1-1 ura3 rad5-G535R*	
W1588	*MATα ade2-1 can1-100 his3-11,15 leu2-3-112 trp1-1 ura3 RAD5*	
MNY1689	*MATα ARS607-ΔHis2-tRNA::URA3-0bp*	This study
MNY1695	*MATα ARS607-ΔHis2-tRNA::URA3-TG_{1-3} 300bp*	This study
MNY1699	*MATα ARS607-ΔHis2-tRNA::URA3-TG_{1-2} 300bp-mod*	This study
MNY1702	*ARS607-ΔHis2-tRNA::URA3-TG0bp GFP-NUP49 leu2 ::LacI**-GFP::LEU2 Chr6int::lacop-lexAop-TRP1 (Chr6int is 272 bp upstream ARS607)*	This study
MNY1709	*ARS607-ΔHis2-tRNA::URA3- TG_{1-3} 300bp GFP-NUP49 leu2 ::LacI**-GFP::LEU2 Chr6int::lacop-lexAop-TRP1 (Chr6int is 272 bp upstream ARS607)*	This study
MNY2217	*ARS607-ΔHis2-tRNA::URA3-TG_{1-3} 300bp sir4 ::TRP1*	This study
MNY1737	*ARS607-ΔHis2-tRNA::URA3-TG_{1-3} 300bp rad5 ::TRP1*	This study
MAJY182	*ARS607-ΔHis2-tRNA::URA3-TG_{1-3} 300bp mre11 ::HIS3*	This study
MNY2210	*ARS607-ΔHis2-tRNA::URA3-TG_{1-3} 300bp ctf18 ::KAN*	This study
MNY1769	*MATalpha ARS607-ΔHis2-tRNA::URA3-0bp NUP2-MNase::HPH*	This study
MNY1768	*MAT**a** ARS607-ΔHis2-tRNA::URA3 TG_{1-3} 300bp NUP2-MNase::HPH*	This study
MNY1885	*ARS607-ΔHis2-tRNA::URA3 TG_{1-2} 300bp-mod NUP2-MNase::HPH*	This study
MNY1862	*MATalpha ARS607-ΔHis2-tRNA::URA3-0bp NUP84-MNase::HPH*	This study
MNY1865	*MATalpha ARS607-ΔHis2-tRNA::URA3 TG_{1-3} 300bp NUP84-MNase::HPH*	This study
MNY1882	*ARS607-ΔHis2-tRNA::URA3 TG_{1-2} 300pb-mod NUP84-MNase::HPH*	This study
MNY1870	*ARS607-ΔHis2-tRNA::URA3 TG_{1-3} 0bp RAP1-MNase::HPH*	This study
MNY1873	*ARS607-ΔHis2-tRNA::URA3 TG_{1-3} 300bp RAP1-MNase::HPH*	This study
MNY1894	*ARS607-ΔHis2-tRNA::URA3 TG_{1-2} 300bp-mod RAP1-MNase::HPH*	This study
MNY 1888	*ARS607-ΔHis2-tRNA::URA3 TG_{1-3} 0pb CDC13-MNase::HPH*	This study
MDY401	*ARS607-ΔHis2-tRNA::URA3 TG_{1-3} 300pb CDC13-MNase::HPH*	This study
MNY1891	*ARS607-ΔHis2-tRNA::URA3 TG_{1-2} 300bp-mod CDC13-MNase::HPH*	This study
MNY213	*ARS607-ΔHis2-tRNA::URA3 TG_{1-2} 300bp RFA1-MNase::HPH*	This study
MAHY219	*ARS607-ΔHis2-tRNA::URA3 TG_{1-2} 300bp-mod RFA1-MNase::HPH*	This study

MNY1773	*MATalpha ARS607-ΔHis2-tRNA::URA3-300bp HIS3::REB1p-MNase-NLS*	This study
DCY6E4	*NUP84-MNase::HPH esc1::TRP1*	This study
DCY6E9	*NUP84-MNase::HPH leu2::mps3Δ75-150-LEU2*	This study
MAHY111	*ARS607-ΔHis2-tRNA::URA3 TG_{1-3} 300bp NUP2-MNase::HPH leu2::mps3Δ75-150-LEU2*	This study
MAHY183	*ARS607-ΔHis2-tRNA::URA3 TG_{1-3} 300bp NUP2-MNase::HPH ars608::HIS3 ars609::TRP1*	This study
MNY1785	*ARS607-ΔHis2-tRNA::URA3 TG_{1-3} 300bp NUP2-MNase::HPH slx8::KanMx*	This study
MNY1826	*ARS607-ΔHis2-tRNA::URA3 TG_{1-3} 300bp NUP2-MNase::HPH rad51::LEU2*	This study
MNY1832	*ARS607-ΔHis2-tRNA::URA3 TG_{1-3} 300bp NUP2-MNase::HPH rad5::TRP1*	This study
MNY1815	*ARS607-ΔHis2-tRNA::URA3 TG_{1-3} 300bp NUP2-MNase::HPH rad59::KanMx*	This study
MAHY28	*ARS607-ΔHis2-tRNA::URA3 TG_{1-3} 300bp NUP2-MNase::HPH mms21ΔCt-myc::TRP1*	This study
MAHY45	*ARS607-ΔHis2-tRNA::URA3 TG_{1-3} 300bp NUP2-MNase::HPH mre11::HIS3*	Dhingra et al 2019
PP3570	*rfa1-4KR (K170, 180, 411, 427)*	This study
MNY1796	*ARS607-ΔHis2-tRNA::URA3 TG_{1-3} 300bp NUP2-MNase::HPH rfa1-4KR (K170, 180, 411, 427)*	Charifi et al. 2021
NEB142-7C	*rad52-K43,44,253R*	This study
MNY1801	*ARS607-ΔHis2-tRNA::URA3 TG_{1-3} 300bp NUP2-MNase::HPH rad52-K43,44,253R*	This study
MNY1810	*ARS607-ΔHis2-tRNA::URA3 TG_{1-3} 300bp NUP2-MNase::HPH uls1::TRP1*	This study
MNY2187	*ARS607-ΔHis2-tRNA::URA3 TG_{1-3} 300bp NUP84-MNase::HPH sir4::TRP1*	This study
DCY6H4	*ARS607-ΔHis2-tRNA::URA3 TG_{1-3} 300bp NUP84-MNase::HPH ctf18::KAN*	This study
DCY6G8	*ARS607-ΔHis2-tRNA::URA3 TG_{1-3} 300bp NUP84-MNase::HPH nup170::KAN*	This study
DCY6H7	*ARS607-ΔHis2-tRNA::URA3 TG_{1-3} 300bp NUP84-MNase::HPH mrc1::NAT*	This study
MNY2214	*ARS607-ΔHis2-tRNA::URA3 TG_{1-3} 300bp NUP84-MNase::HPH mrc1-AQ::LEU2*	Petela et al., 2018

K20571	*scc2-45 L545P D575G::NAT SCC1-Pk9::TRP1*	This study
MNY2199	*ARS607-ΔHis2-tRNA::URA3 TG$_{1-3}$ 300bp NUP84-MNase::HPH scc2-45 L545P D575G::NAT*	This study
MPY22	*ade1::NAT ARS922-URA3-TG$_{1-3}$ 300bp-ADE2*	This study
MPY25	*ade1::NAT ARS922-URA3-TG$_{1-3}$ 300bp-mod-ADE2*	This study
MPY37	*ade1::NAT ARS922-URA3-TG$_{1-3}$ 300bp-ADE2 rfa1-D228Y*	This study
MPY33	*ade1::NAT ARS922-URA3-TG$_{1-3}$ 300bp-ADE2 rad5::TRP1*	This study
MPY98	*ade1::NAT ARS922-URA3-TG$_{1-3}$ 300bp-ADE2 ctf18::KAN*	This study
MPY70	*ade1::NAT ARS922-URA3-TG$_{1-3}$ 300bp-ADE2 sir4 ::TRP1*	This study
MAHY309	*ade1::NAT ARS922-URA3-TG$_{1-3}$ 300bp-ADE2 mre11::HIS3*	This study
MNY1830	*MAT**a**/MATa EST2/est2::LEU2 MMS21/mms21ΔCt-myc ::TRP1*	This study
MAHY377	*MAT**a**/MATa EST2/est2::LEU2 CTF18/ctf18 ::KAN*	This study

Yeast strains used in this study. Strains are derivatives of W303-1A (*MAT***a** *BAR1 LYS2 ade2-1 can1-100 ura3-1 his3-11,15 leu2-3, 112 trp1-1 rad5-535*) (Thomas and Rothstein, 1989) or W1588 (*RAD5*).